Fine Sediment Trapping in the Penobscot River Estuary

Author: Christie A. Hegermiller

BOSTON COLLEGE
College of Arts and Sciences

The thesis of: Christie A. Hegermiller

Title: Fine Sediment Trapping in the Penobscot River Estuary

Submitted to the Department of: Earth and Environmental Sciences

In partial fulfillment of the requirement for the degree of:
Bachelor of Science with Departmental Honors

In the College of Arts & Sciences, has been read and approved by the Committee:

Advisor Gail C. Kineke, Ph.D.

Member

Date

Fine Sediment Trapping in the Penobscot River Estuary

a senior thesis
by

Christie Hegermiller

May 2011

Department of Earth and Environmental Sciences
Boston College

Abstract

The Penobscot River Estuary is heavily contaminated with mercury; previous studies indicate maximum mercury concentrations of 4.6 ppm within the Frankfort Flats reach. The transport and trapping of this contaminant is linked to the transport and trapping of fine sediment within the estuary. Hydrographic and flow measurements, coupled with a spatial and temporal characterization of the bottom sediments, were performed during and following the freshet in 2010 to determine the mechanisms driving sediment transport and trapping within the estuary. The Penobscot River likely has a turbidity maximum associated with the landward extent of the salinity intrusion that is positioned over the Frankfort Flats reach during average discharge and tidal conditions. This turbidity maximum may be responsible for a patch of fine sediments in the Frankfort Flats reach in an otherwise coarse-grained bed. Additional transport and trapping of fine sediments within this reach is the result of secondary circulation driven by centripetal acceleration around meanders in the channel. Close proximity of meanders at Frankfort Flats, within ~5 km, creates opposite secondary circulation of magnitude ~0.2 m/s during flood and ebb conditions.

Acknowledgements

This thesis would not have been possible without the constant guidance, support, and patience from my advisor, Gail C. Kineke. I am indebted to you for your direction and love over these past three years. You have become far more than my academic advisor and I could write pages on what you have done for me. Thank you so much for all of this and more, namely your patience, which I know I have stretched thin over the years.

Thank you to Rocky Geyer for your guidance, for putting up with my constant questions, and for knowing me better than I know myself. Luckily, I won't have to make the Boston-Cape drive too often anymore. Thank you to Dave Ralston, Dan Belknap, Jim Churchill, Jay Sisson, and the Maine Maritime crew for their help in the field and with data processing.

A huge thank you to Mike Cuttler and Dylan Anderson, who mentally and emotionally saved me too many times to count. You have quickly become two of my closest friends and I can't wait to get to work with you this summer and hopefully more in the future. I was lucky to be surrounded by your intelligence and humor. Another huge thank you to my roommates and friends, who dealt with my frazzled self and my books and papers perpetually all over the kitchen table. I couldn't have finished without your support and love. And of course, thank you to my mom, who received too many 5 am phone calls and always knew best how to ease my nerves.

Table of Contents

List of Tables and Figures

Figure 9: Spatial surveys were conducted in April, May, and June 2010 over four lines: Verona, Orland, Frankfort Flats, and a large-scale survey. The large-scale survey is not shown on this figure. Data from the Frankfort Flats survey line are presented in this paper.

Figure 10: The top figure displays surface salinity in blue and bottom salinity in green from the Verona mooring and tripod from April through June. The bottom figure shows the water surface height in meters, which is indicative of the tidal cycle. Notable spring and neap tides are marked.

Figure 11: The top figure displays surface salinity in blue and bottom salinity in green from the Winterport mooring and tripod from April through June. The bottom figure shows the water surface height in meters, which is indicative of the tidal cycle. Notable spring and neap tides are marked.

Figure 12: Grain size analysis results for April grab stations. 'Fine' is defined as finer than 0.0625 mm.

Figure 13: Grain size analysis results for May grab stations. 'Fine' is defined as finer than 0.0625 mm.

Figure 14: Grain size analysis results for June grab stations. 'Fine' is defined as finer than 0.0625 mm.

Figure 15: Bathymetry of the Frankfort Flats reach of the lower Penobscot River Estuary. Note that the channel meanders around a right-hand bend and a left-hand bend in this reach going upstream. (U.S. Geological Survey)

Figure 16: The salinity structure (psu), along-channel velocity (m/s), across-channel velocity (m/s), and suspended-sediment concentration (mg/L) during maximum flood in May along the Frankfort Flats survey line. For along-channel, positive velocities indicate flooding and negative velocities indicate ebbing. For across-channel, positive velocities indicate flow to the left and negative velocities indicate flow to the right, also indicated by the arrows. The black square marks the location of station WH 2.

Figure 17: The salinity structure (psu), along-channel velocity (m/s), across-channel velocity (m/s), and suspended-sediment concentration (mg/L) during maximum flood in June along the Frankfort Flats survey line. For along-channel, positive velocities indicate flooding and negative velocities indicate ebbing. For across-channel, positive velocities indicate flow to the left and negative velocities indicate flow to the right, also indicated by the arrows. The black square marks the location of station WH 2.

Figure 18: The salinity structure (psu), along-channel velocity (m/s), across-channel velocity (m/s), and suspended-sediment concentration (mg/L) during maximum ebb in May along the Frankfort Flats survey line. For along-channel, positive velocities indicate flooding and negative velocities indicate ebbing. For across-channel, positive velocities indicate flow to the left and negative velocities indicate flow to the right, also indicated by the arrows. The black square marks the location of station WH 2.

Figure 19: The salinity structure (psu), along-channel velocity (m/s), across-channel velocity (m/s), and suspended-sediment concentration (mg/L) during maximum ebb in June along the Frankfort Flats survey line. For along-channel, positive velocities indicate flooding and negative velocities indicate ebbing. For across-channel, positive velocities indicate flow to the left and negative velocities indicate flow to the right, also indicated by the arrows. The black square marks the location of station WH 2.

Figure 20: Salinity structure in April, May, and June, showing the landward progression of the salt wedge after being pushed seaward during the April freshet. The black squares are kilometers ~15, 27 and 31 are the Verona, Frankfort Flats, and Winterport stations, respectively.

Figure 21: The near-bottom velocity at the Verona tripod as referenced to the tidal hour (a). Suspended-sediment concentration at the Verona tripod as referenced to the tidal hour (b). Maximum turbidity occurs during late ebb. Tidal Hour 0 is low water at Portland, ME.

Figure 22: The near-bottom velocity at the Winterport tripod as referenced to the tidal hour (a). Suspended-sediment concentration at the Winterport tripod as referenced to the tidal hour (b). Maximum turbidity occurs during late ebb. Tidal Hour 0 is low water at Portland, ME.

Figure 23: Near-bottom suspended-sediment concentrations at the Verona and Winterport tripods and the tidal amplitude at Frankfort Flats to show correlations in resuspension and the spring-neap and daily tidal cycles.

Figure 24: Grab sampling locations in the Frankfort Flats reach of the Penobscot River Estuary in June. The ADCP and CTD Frankfort Flats survey line is superimposed on the grab locations. The median grain sizes of sediments collected at sites WH 0, WH 1, and WH 5 were used to compare the shear stress provided by the flow at the sites and the critical shear stress of the sediments to determine if sediments are transported by tidal currents or are lag deposits.

Figure 25: Excess u100*|u100| throughout the tidal cycle with reference to the critical u100*|u100| for the median grain size of sediment at WH 1.

Figure 26: Excess u100*|u100| throughout the tidal cycle with reference to the critical u100*|u100| for the median grain size of sediment at WH 0.

Figure 27: Excess u100*|u100| throughout the tidal cycle with reference to the critical u100*|u100| for the median grain size of sediment at WH 5.

Figure 28: Instantaneous flux profiles in (mg/L*m/s) at maximum flood and ebb currents in May and June in the thalweg along the Frankfort Flats transect. The direction of the flux is determined by the direction of the across-channel velocity. Therefore, negative values represent flux to the east, when looking upstream, and positive values represent flux to the west from the same orientation.

Figure A1: Mean velocity profiles in the thalweg during April throughout the tidal cycle. Tidal hour is noted at the top of each plot.

Figure A2a: Mean velocity profiles in the thalweg during May throughout the tidal cycle. Tidal hour is noted at the top of each plot.

Figure A2b: Mean velocity profiles in the thalweg during May throughout the tidal cycle. Tidal hour is noted at the top of each plot.

Figure A3a: Mean velocity profiles in the thalweg during June throughout the tidal cycle. Tidal hour is noted at the top of each plot.

Figure A3b: Mean velocity profiles in the thalweg during June throughout the tidal cycle. Tidal hour is noted at the top of each plot.

Figure A4a: Mean velocity profiles at site WH 1 throughout the tidal cycle. Tidal hour is noted at the top of each plot.

Figure A4b: Mean velocity profiles at site WH 1 throughout the tidal cycle. Tidal hour is noted at the top of each plot. Maximum velocity at one meter above the bed occurs during tidal hour ~11.00.

Figure A5a: Mean velocity profiles at site WH 0 throughout the tidal cycle. Tidal hour is noted at the top of each plot. Maximum velocity at one meter above the bed occurs during tidal hour ~3.60.

Figure A5b: Mean velocity profiles at site WH 0 throughout the tidal cycle. Tidal hour is noted at the top of each plot. The tide continues to change from ebb to flood at hour ~9.98.

Figure A6a: Mean velocity profiles at site WH 5 throughout the tidal cycle. Tidal hour is noted at the top of each plot. Maximum velocity at one meter above the bed occurs during tidal hour ~4.38.

Figure A6b: Mean velocity profiles at site WH 5 throughout the tidal cycle. Tidal hour is noted at the top of each plot. Maximum velocity at one meter above the bed occurs during tidal hour ~11.

Introduction

Estuaries are commonly regions of contaminant accumulation because of elevated suspended-sediment concentrations and sediment-trapping mechanisms generated by the interaction of estuarine circulation and tidal exchange (Dyer, 1997). Contaminants bind to the fine, cohesive sediments that are prevalent in estuaries and are eroded, transported, and deposited according to the dynamics of sediment transport within estuaries.

The Penobscot River Estuary is located approximately 130 km north of Portland on Maine's coastline (Figure 1). It is a heavily contaminated estuary that is currently undergoing several restoration projects (Penobscot River Synthesis Project (PRSP), 2005). The Penobscot River basin was formed during the last glaciation and its contamination dates to the 1800s. The Penobscot River was predominately used by the lumber industry in the mid-1800s. Approximately 4% of all logs driven down the river sank before reaching their destination (Davies, 1972; PRSP, 2005). Lumber companies, and later pulp and paper industries, dumped sawdust, edgings, and bark into the river until as late as 1950. According to two studies conducted in 1967 and 1969, sawdust accounted for as much as 15% of river sediments at certain locations in the lower reaches of the estuary (Haefner, 1967; Shorey, 1969; PRSP, 2005). Additionally, 47 leather and textile plants operated in the lower Penobscot by 1960 (Maine Department of Economic Development, 1957; PRSP, 2005). Discharge from these facilities, combined with raw sewage and discharge from poultry slaughterhouses, rendered the river downstream of Bangor unusable for fishing, consumption, or even recreation (U.S. Federal Water Pollution Control Administration, 1967; PRSP, 2005).

From 1967 to 2000, a HoltraChem facility along the river used mercury to make chlorine and other chemicals for the paper industry (PRSP, 2005). This company discharged mercury to the river and the surrounding lands until they were investigated in the 1990s. Previous studies have shown sediment mercury concentrations as high as 4.6 ppm in some samples from sediments in Frankfort Flats (Livingston, 2000; PRSP, 2005). The state has warned that fish caught in the Penobscot are contaminated with mercury, dioxins, and PCBs.

The Penobscot is the largest river in Maine and the second largest river in New England. It drains an area of 22,252 km^2, which accounts for more than one-quarter of

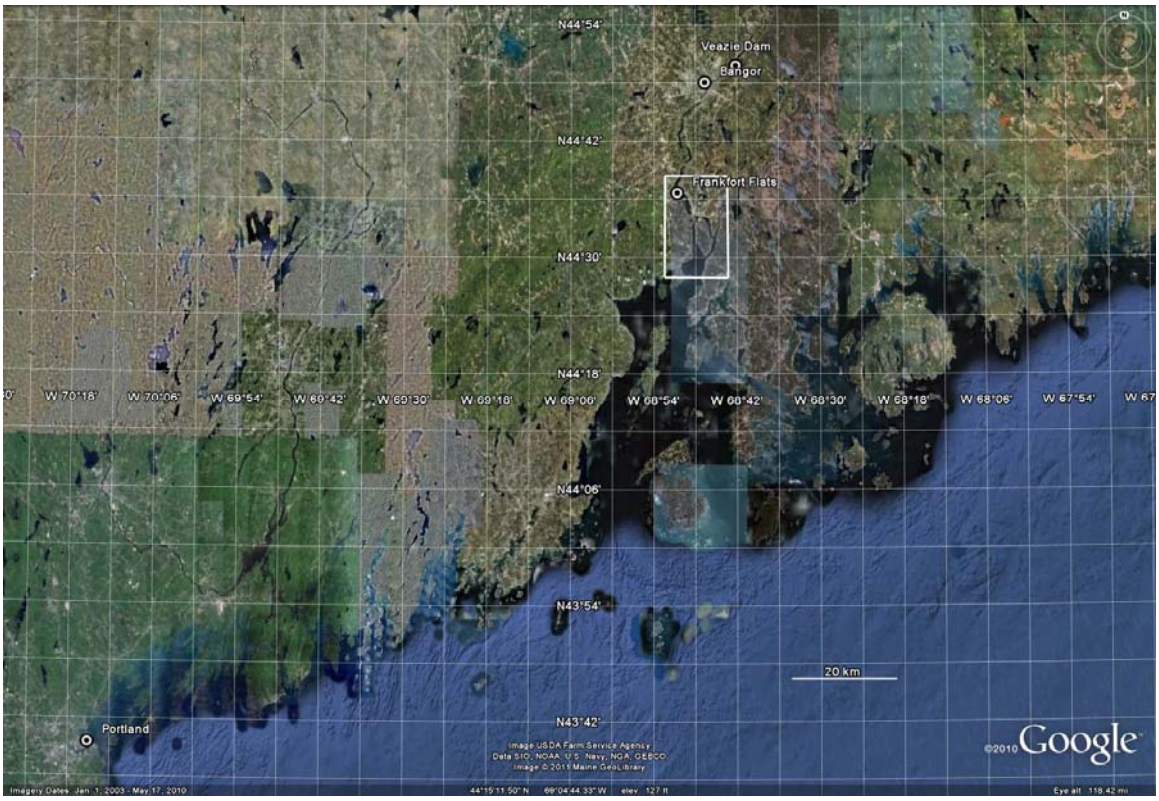

Figure 1. The southern coastline of Maine and marked locations of Portland, Frankfort Flats, and Bangor. The study area is boxed in white. (Google Earth Imagery)

the land of Maine (PRSP, 2005). The average discharge is approximately 402 m^3/s (PRSP, 2005). The river is tidally influenced to Bangor, with marine waters extending to Winterport during low flow conditions (PRSP, 2005). The estuary is classified as partially mixed and is sediment limited (PRSP, 2005).

This history of contamination is related to the physical processes responsible for the trapping of fine sediments. In order to understand the transport and deposition of contaminants within the Penobscot River, it is necessary to document and determine the mechanisms of sediment transport and trapping within the estuary. The purpose of this study is to identify areas of fine-grained sediment accumulation and the processes controlling deposition in the Frankfort Flats reach of the Penobscot River, which was accomplished through spatial and temporal analysis of bottom sediment characteristics, analysis of along- and across-channel circulation patterns, and observation of water column structure in regards to salinity and suspended-sediment concentration.

Background

Estuaries are ephemeral features, in geologic time, that exist at the boundaries between the coastal ocean and riverine terrestrial domains. Following scouring during the Pleistocene and the flooding of these valleys in post-glacial years, estuaries presently populate the earth as complex and well-developed environments (Dyer, 1997). A common definition identifies three key attributes of an estuary: a semi-enclosed coastal body of water which has free connection to the open sea, which extends into the river as far as the limit of tidal influence, and within which sea water is measurably diluted with fresh water derived from land drainage (Cameron and Pritchard, 1963; Dyer, 1997).

The influence of tides is important in determining the internal hydrographic structures and physical processes that will be prevalent in an estuary. Semi-diurnal tidal cycles are distorted by bathymetry-induced friction upon entering estuaries, producing asymmetry in the tidal curve (Dyer, 1997). Whether a regime is flood-dominated or ebb-dominated affects the direction of net sediment transport.

Estuarine Circulation

Water-column structure and governing processes vary in estuaries because they are subjected to a combination and interaction of marine and fluvial processes. Fresh water input and salt water encroachment are the main drivers of estuarine circulation (Valle-Levinson, 2010). As fresh water flows seaward over denser salt water, a vertical salinity gradient is created. A horizontal salinity gradient also exists in estuaries because of fresh water input: salinity decreases from the ocean towards the head of the estuary (Geyer, 2010). Although density is a function of salinity, temperature, and suspended-sediment concentration, the salinity range in estuaries is significantly greater than the temperature range. Therefore, in estuaries with low to moderate suspended-sediment concentration, density differences are dominated by salinity. At the halocline, or region of greatest vertical salinity gradient, turbulence resulting from velocity shear acts to draw salt water into the seaward flowing fresh water (Dyer, 1997). This process is called entrainment. In order to compensate for the loss of salt water from the bottom layer, there is a landward flow of the salt water in the lower water column. The strength of this circulation is dependent on the strength of the fresh water outflow and the degree of mixing by tidal currents (Figure 2; Geyer, 2010). Estuarine circulation is a residual flow

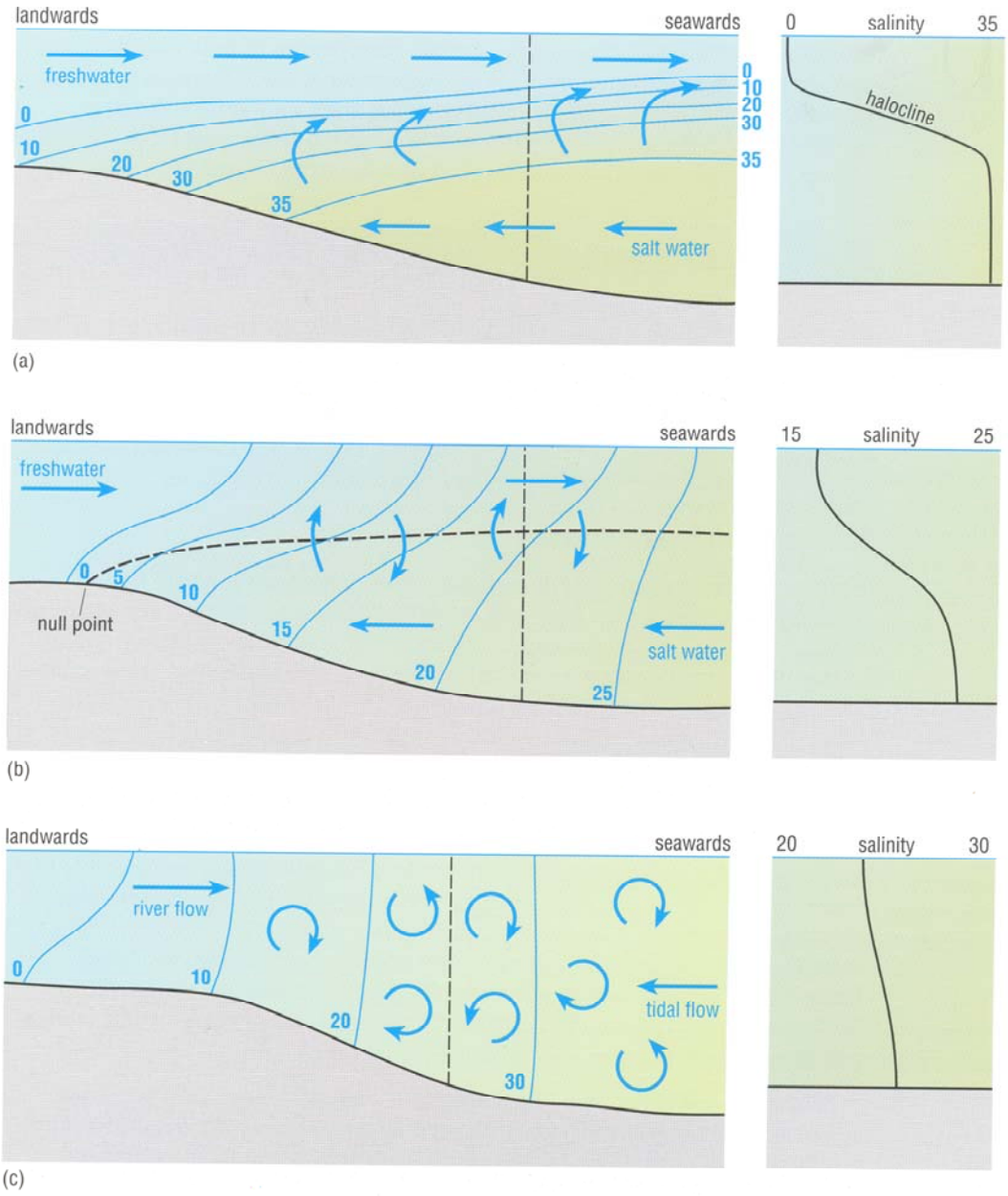

Figure 2. The dynamics and processes controlling estuarine circulation in salt-wedge estuaries (a), partially-mixed estuaries (b), and well-mixed estuaries (c). Arrows represent flow, mixing, and entrainment and contours are salinity. (Brown et al., 1999)

in the sense that flow at any given time within an estuary is usually dominated by tidal currents. However, if the flow is tidally averaged, the estuarine circulation is distinguishable.

Secondary Circulation

An additional circulation occurs in estuaries that is normal to the velocity of the main flow, or, more simply, normal to the channel orientation. This secondary circulation is generally less than 10% of the magnitude of the along-channel flow, but can be equally as important in driving dispersion within a system (Chant, 2010). In meandering rivers, flow traveling around a bend experiences a centripetal acceleration towards the outside of the bend. Within the fast-moving surface waters, a net outward flow piles water at the outer edge of the bend. The slower-moving bottom waters experience a net inward flow, requiring a barotropic force to balance the pressure gradient (Dyer, 1997). The piled surface waters downwell as the bottom waters upwell, driving a helical lateral flow (Figure 3; Chant, 2010). The centripetal acceleration always acts in the same direction around a particular bend regardless of the direction of the along-channel flow and, therefore, the secondary circulation due to curvature will always be in the same direction around a particular bend. Secondary circulation due to curvature will flow in a counter-clockwise direction around a left-handed bend and clockwise around a right-handed bend from the same orientation (Dyer, 1997). Secondary circulation is also generated in estuaries by Coriolis acceleration and differential advection of longitudinal salinity gradients (Chant, 2010).

Salinity Structure

In estuaries where river flow is dominant, fresh water draining seaward over the surface of the bottom salt water layer creates a salt wedge (Dyer, 1997). The salt wedge is pushed downstream by the river flow until the slope of the halocline is sufficient to balance the velocity shear (Dyer, 1997). The process of entrainment is highly influential in driving estuarine circulation in salt wedge estuaries. As tides become more dominant in the regime, increased turbulence promotes greater mixing between fresh and saline waters, creating a partially-mixed estuary (Figure 2). Turbulent mixing causes greater entrainment and the loss of salt water to the seaward flowing fresh water is increased. This enhances estuarine circulation in partially-mixed estuaries because it requires a

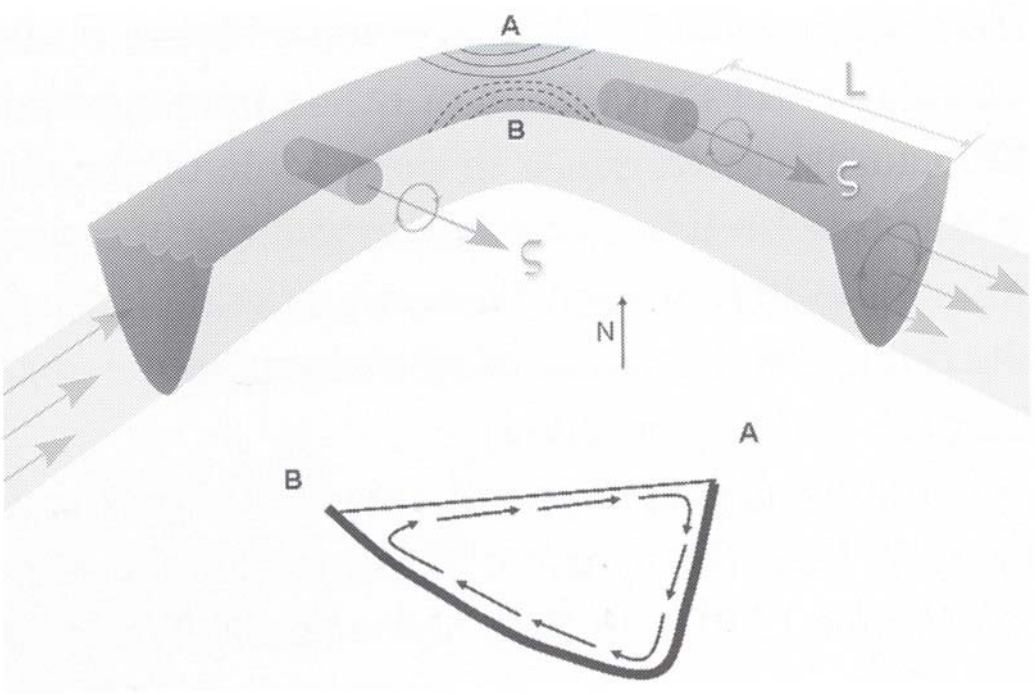

Figure 3. The mechanism that creates secondary circulation due to curvature. Lines at the bend represent the elevated (solid) and lowered (dashed) sea level. ζ symbolizes the direction of the relative vorticity vector and L corresponds to the length scale of the duration of secondary circulation beyond the bend. (Chant, 2010)

stronger landward flow of bottom salt water. Most partially-mixed estuaries are mesotidal (tidal range between 2 and 4 m) (Davies, 1964; Dyer, 1997). A well-mixed estuary occurs when the tidal range is significantly greater than the water depth and tides are strong enough to mix the entire water column, creating a vertically homogenous system (Dyer, 1997).

Estuarine Turbidity Maximum

Fluvial sediment supply and the convergence of fresh and salt water make estuaries an effective trap for fine sediments. At the maximum vertical salinity gradient, a level of no motion exists where mean flow is zero (Dyer, 1997). Where this level of no motion reaches the bed, often at the head of a salt intrusion, there is a convergence of bottom velocities, called a null point (Figure 4) (Dyer, 1997). Fine sediments tend to become trapped in this zone, near the landward extent of the salinity intrusion, resulting in concentrations of suspended sediments higher than elsewhere within the estuary, creating a region known as the turbidity maximum. In mesotidal estuaries, suspended-sediment concentrations within the turbidity maximum are typically 100-200 mg/L and sediments can experience a residence time of greater than one year (Dyer, 1997).

The position of the turbidity maximum within an estuary varies with river discharge (Uncles and Stephens, 1989; Dyer, 1997). Higher discharge shifts the turbidity maximum seaward. Mass export of sediments may only occur during large discharge events that can push the turbidity maximum to the mouth of the estuary, or even flush it out of the system (Geyer et al., 2001). If the sediment supply is greater than the amount of sediment that can remain in suspension, deposition occurs beneath the turbidity maximum as a swath of mobile mud (Traykovski et al., 2004). The strength of the turbidity maximum is dependent on the sediment supply, the strength of the estuarine circulation, and the settling velocity (Geyer, 1993). Additionally, variations in the turbidity maximum can occur between spring and neap tidal cycles. During spring tides, increased shear stress at the bed is able to erode a greater quantity of sediment and increased turbulence can keep sediments in suspension (Dyer, 1997). Trapping is also enhanced at the turbidity maximum with increases in flocculation and stratification, which both promote settling of sediments in the region of convergence near the landward

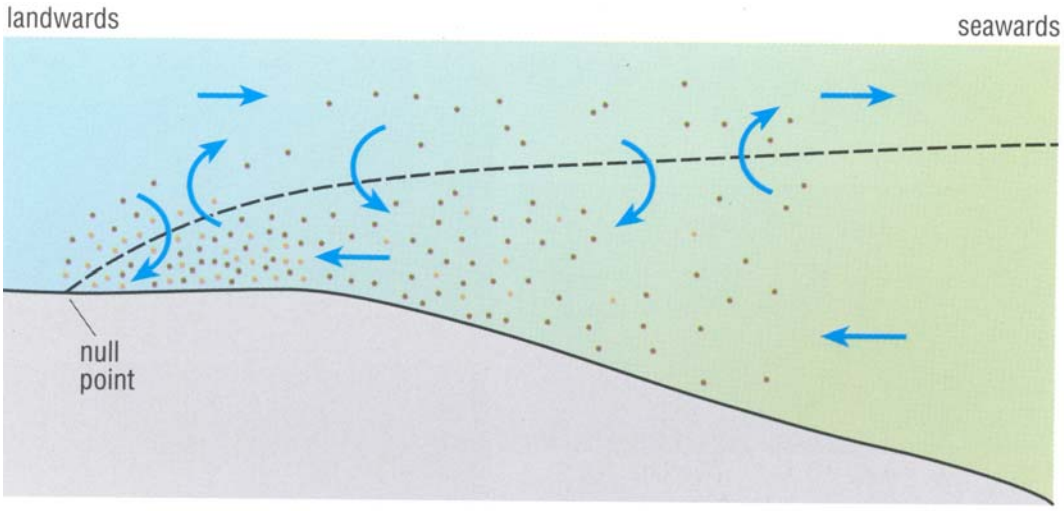

Figure 4. A schematic representation of the turbidity maximum in a partially-mixed estuary, where vertical arrows represent turbulent mixing and horizontal arrows represent flow of the bottom and surface waters. The dashed line represents the location of the halocline in the water column. Suspended sediment is depicted as brown dots and is highly concentrated at the landward extent of the salt intrusion (dashed line). (Brown et al., 1999)

limit of the salinity intrusion (Geyer, 1993). Flocculation forms aggregates of clay particles and stratification dampens turbulent mixing within the water column.

Sediments in Estuaries

Estuaries predominantly transport fine sediments because they are far-removed from the sediment source. Fine sediments are a mixture of cohesive silt and clay particles and often contain varying degrees of organic material. The cohesive properties of fine sediments are largely due to the clay fraction of the sediment, but are also influenced by the organic content (Partheniades, 2009). Clays are silicates of aluminum, magnesium, or iron. Clay particles have negative charges on their faces and positive charges on their sides. Due to the platy structure of clay particles, the faces of the particles dominate, giving them a net negative charge. Depending on the fluid in which these particles interact, attractive or repulsive interparticle forces can exist. However, attractive forces are induced in the presence of an electrolyte, such as salt, within a fluid (Partheniades, 2009). Brownian motion, which is random motion in all directions caused by thermal activity of water molecules, causes sediment particles to collide (Partheniades, 2009). When particles collide, the attractive interparticle forces make them stick. This process, called flocculation, can create large flocs in the water column, which have a greater settling velocity than individual particles. Organic matter can also promote flocculation. The cohesive nature of fine sediments is important not only for mechanisms of suspension, but also influences erodability and critical shear stress for resuspension.

Shear Stress

A fluid flowing over the surface of the sea bed produces a shear stress that acts on the bed. Shear stress is a function of viscosity and the average velocity gradient (Brown et al., 1999). A quantity known as the shear velocity (u_*) has been defined as:

$$u_* = \sqrt{\frac{\tau_0}{\rho}} \qquad (1)$$

$$\tau_0 = \rho u_*^2 \qquad (2)$$

where τ_0 is bed shear stress and ρ is the density of the fluid (Brown et al., 1999). The shear velocity is typically an order of magnitude smaller than measured mean velocities (Brown et al., 1999).

Sternberg (1972) outlines two methods for determining boundary shear stress from field measurements. In the bottom boundary layer, velocity increases logarithmically with height above the bed and is described by the Karman-Prandtl velocity profile equation, or the "Law of the Wall," that relates change in velocity with height above the bed to the stress at the bed, with u_* as a convenient proxy for boundary shear stress:

$$\frac{u}{u_*} = \frac{1}{\kappa} ln\left(\frac{z}{z_0}\right) \quad (3)$$

where κ is the Von-Karman constant equal to 0.4, z_0 is the roughness length, z is height above the bed, and u is the average current velocity at z (Figure 5). The roughness length is related to the grain size of bed sediments and bedforms. This technique requires at least three measurements of velocity within the boundary layer.

The Quadratic Stress Law utilizes a drag coefficient (C_{100}) and a velocity measurement at 100 cm above the bed (u_{100}) to determine shear velocity and shear stress (Sternberg, 1972):

$$\tau_0 = C_{100}\rho\bar{u}_{100}^2 \quad (4)$$

$$u_* = C_{100}^{1/2}\bar{u}_{100} \quad (5)$$

The drag coefficient is related to the bed roughness and to the roughness length. Sternberg suggests that the drag coefficient approaches a constant for various grain sizes. A compilation of data suggests that C_{100} is equal to 3.0 x 10^{-3} for sand and gravel beds and decreases with decreasing particle size (Sternberg, 1972).

Bed sediments require a critical shear stress (τ_c) to initiate motion, also called the yield stress. While the critical shear stress for non-cohesive sediments increases with

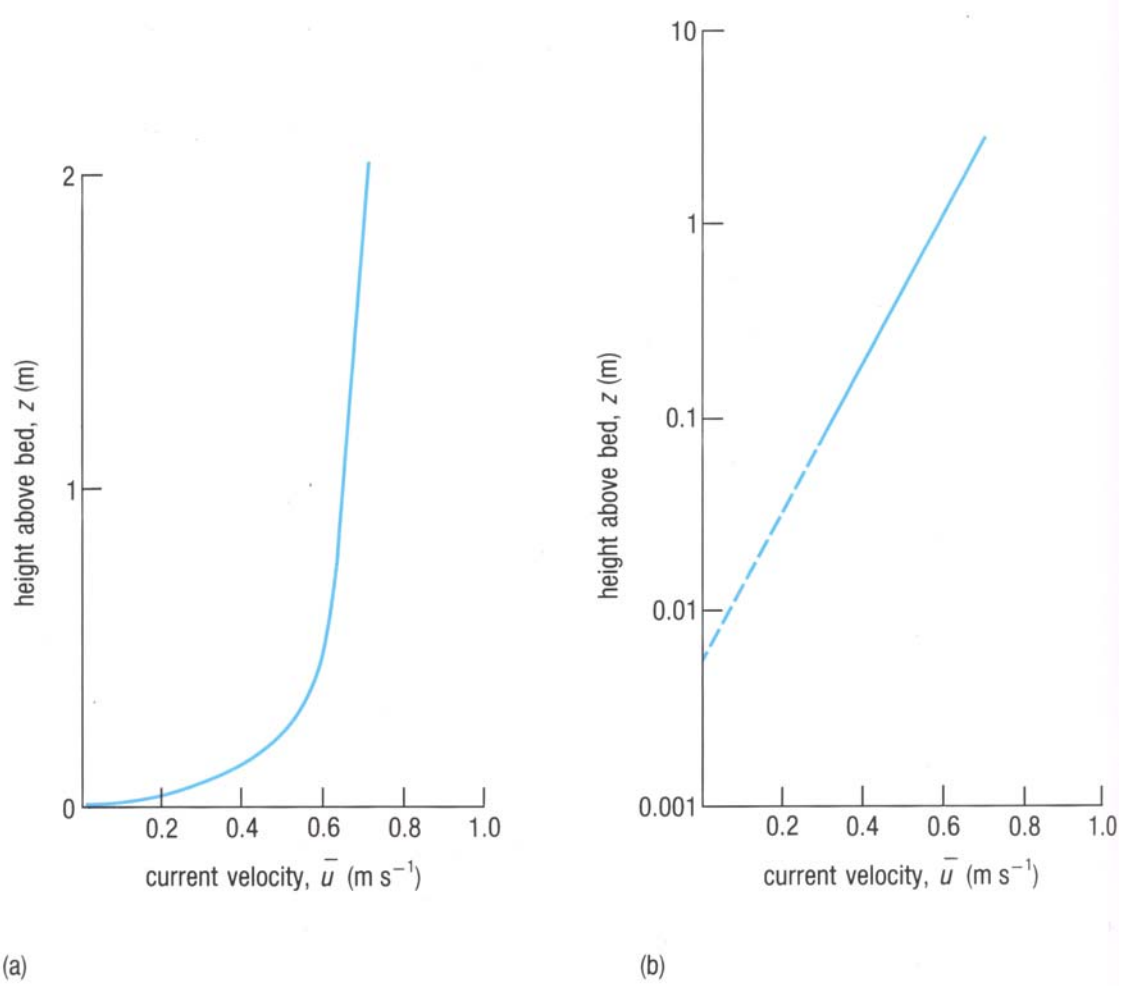

Figure 5. An ideal velocity profile for flow over the sea bed (a) and the same velocity profile plotted using a logarithmic vertical axis (b), which is described by the "Law of the Wall" equation. (Brown et al., 1999)

increasing grain size as expected, the relationship between yield strength and grain size in cohesive sediments is less intuitive. As sediments become increasingly cohesive and compacted with decreasing grain size, critical shear stress increases. Erosion of cohesive, but uncompacted sediments requires shear stresses equivalent to those needed to move fine gravel (Brown et al., 1999). Critical shear stress increases as compaction of sediments increases with time. Biological production and organic matter can also have varying effects on resistance to erosion. The critical shear stress for most muddy sediments falls within the large range of 0.5 to 5.0 kg m/s^2 (Partheniades, 2009).

Methods

The study area for this project includes the lower reaches of the Penobscot River Estuary (Figure 6). The lower main stem is intersected by Marsh River at a stretch known as Frankfort Flats. The lower river is also split by Verona Island and connected to the Orland River at the eastern and southern ends of this island. Previous research concluded that significant sawdust accumulation occurred in the Frankfort Flats stretch of the river, suggesting that mechanisms exist here that could trap fine sediments and the contaminants they carry (PRSP, 2005). Experiments were conducted throughout the lower estuary between April and June 2010 to document flow conditions, water column and salinity structure, suspended-sediment distribution, and bed characteristics during and following the freshet (Figure 7).

Bed Characteristics

A side-scan survey was completed in June 2010 over the study area and processed by Dr. Dan Belknap of the University of Maine. The spatial and temporal variability of the bed was determined through grain size analysis of bottom sediment samples. Grab samples were collected on April 2, May 12, and June 25 using a sampler tripped at the bed by a spring-released pin off the stern of the R/V *Friendship* (Maine Maritime Academy). Samples were collected at five locations each month (Fort Point, Verona, Indian Point, Frankfort Flats, and Winterport). Additional locations were sampled in May and June (Figure 6). In June, the locations of additional samples were determined based on side scan imagery. Five samples were collected in April, seven in May, and 23 in June (Figure 8). Samples were described and photographed directly following collection. After transportation from the field, samples were stored at 4˚C until initial analyses.

A summary of the analyses performed on each grab sample can be found in Table 1. The organic content of each sample was estimated based on loss on ignition procedures. Given the high organic content of some samples, between 80 and 90%, it was not feasible to perform analyses of the inorganic sediments of these samples. Additionally, after loss on ignition procedures, there was not enough sediment remaining for further analyses of the April Verona station. Samples were wet-sieved for 2, 3, and 4 phi (0.25, 0.125, and 0.0625 mm, respectively) fractions. After drying, loss on ignition

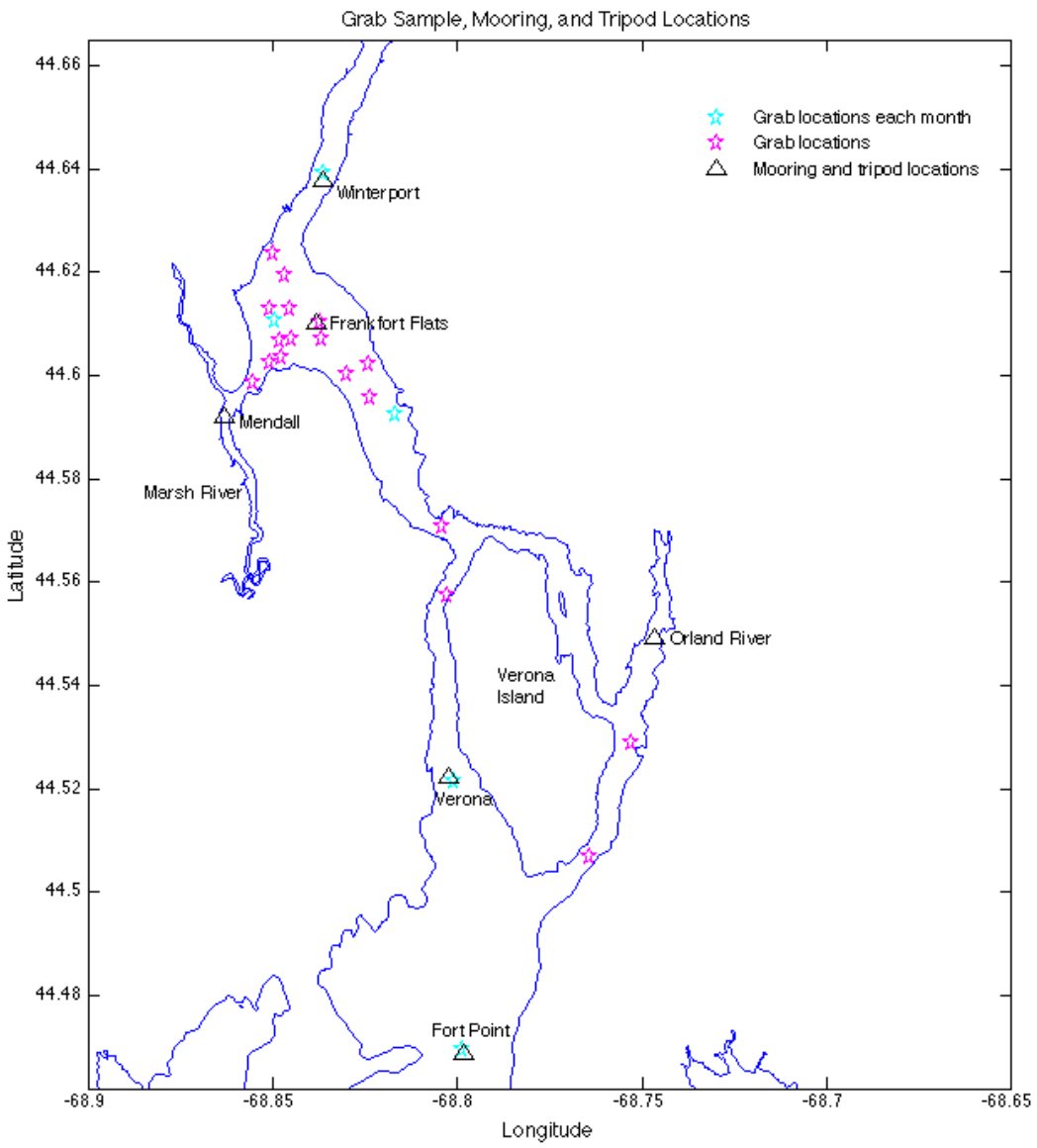

Figure 6. A site map of the study area of the lower Penobscot River Estuary. Locations of grab samples and tripods are marked.

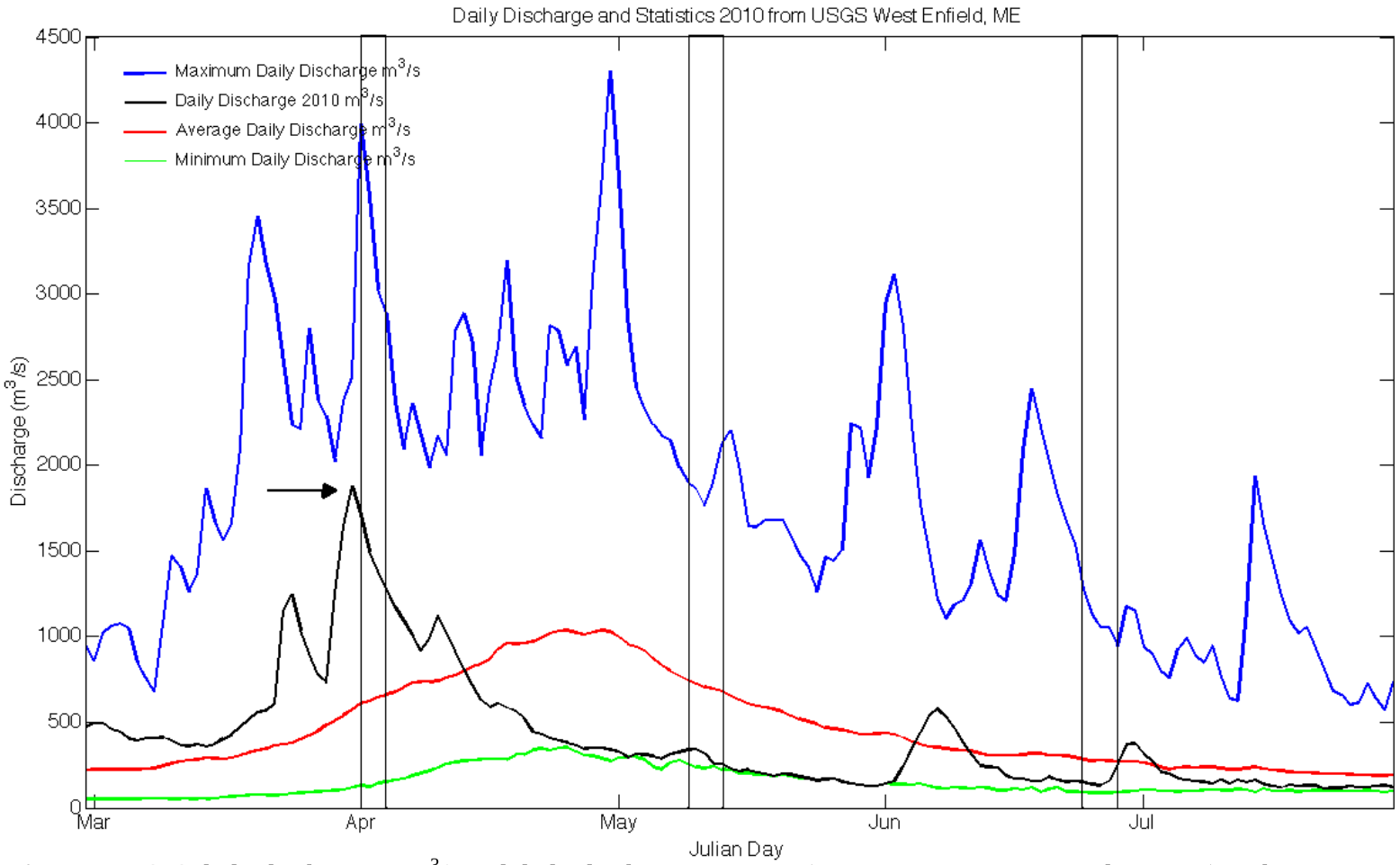

Figure 7. 2010 daily discharge in m^3/s and daily discharge statistics (maximum, minimum, and average) at the West Enfield dam, north of Bangor, from 1902 to 2010. The days of the field experiments in April, May, and June are boxed. The April field experiment occurred during the 2010 spring freshet. The arrow indicates the peak of the 2010 freshet. (U.S. Geological Survey)

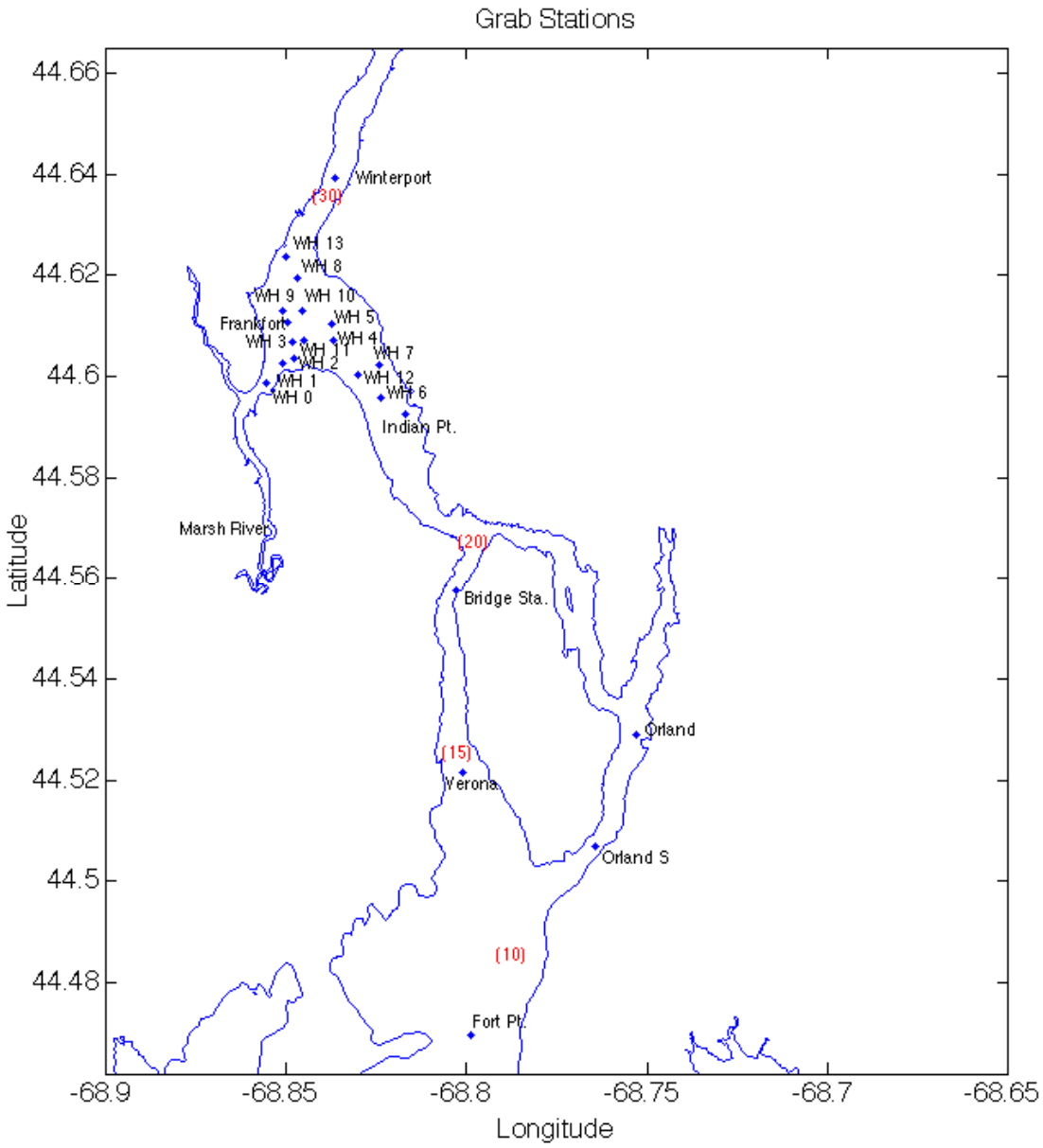

Figure 8. Grab station locations for April, May, and June. Numbers in red denote kilometers from Penobscot Bay.

Month	Day	Hour	Minute	Lat Dec Deg	Lon Dec Deg	Sample	Description	Sedigraph	Sieve	Sieve 2X	d50 (phi)	% Fines	Avg % Org	Comments
4	2	10	53	44.639	68.837	Winterport	gravel		x		<2	2.821	1.345	
4	2	11	16	44.610	68.850	Frankfort Flats			x		>4	77.422	27.968	
4	2	11	38	44.592	68.817	Indian Pt.	very watery		x		>4	42.044	35.748	
4	2	13	41	44.468	68.797	Fort Pt.	thick mud		x		>4	78.386	19.057	
4	2	12	49	44.521	68.803	Verona	big rocks						3.879	Only enough sample for LOI
5	12	8	20	44.468	68.797	Fort Pt.	thick mud		x		>4	84.013	13.402	
5	12	11	0	44.639	68.837	Winterport	gravel		x		<2	2.225	2.062	
5	12	10	45	44.610	68.850	Frankfort Fl.	organics		x		>4	84.831	34.686	
5	12			44.571	68.804	Bucksport			x		>4	42.805	28.803	
5	12			44.557	68.804	Bridge Sta.			x		<2	25.120	6.994	
5	12	8	50	44.521	68.803	Verona			x		2.796	21.465	3.190	
5	12			44.592	68.817	Indian Point	woodchips						88.206	Predominantly organic matter
6	25			44.469	68.799	Fort Pt.	fines, rare gravel	x	x		>4	82.237	18.969	
6	25			44.611	68.850	Frankfort Fl.	firm mud	x	x		>4	79.496	16.335	
6	25			44.507	68.765	Orland S	woodchips		x				79.372	Predominantly organic matter
6	25			44.529	68.753	Orland	coarse silt, fine sands		x		3.589	20.878	9.966	
6	25			44.522	68.801	Verona	heterogeneous mud		x		2.878	27.229	4.927	
6	25			44.557	68.803	Bridge Sta.	consolidated muds	x	x		>4	47.080	22.714	Inconsistent over April-June
6	25			44.557	68.803	Bridge Sta.	mud		x		>4	92.843	33.412	Inconsistent over April-June
6	25			44.571	68.806	Bucksport	NOTHING							Three attempts - no grab sample
6	25			44.593	68.817	Indian Pt.	coarse sands, gravel		x		<2	3.682	2.062	Inconsistent over April-June
6	25			44.599	68.855	WH 0	coarse sands, gravel, shells		x	x	<0	2.354	1.265	
6	25			44.602	68.851	WH 1	cohesive muds		x		2.920	35.070	7.813	
6	25			44.603	68.848	WH 2	perfect mud	x	x		>4	90.660	27.747	
6	25			44.607	68.848	WH 3	mud, twigs, woodchips	x	x		>4	61.323	20.372	
6	25			44.607	68.837	WH 4	heterogeneous		x	x	0.179	10.862	3.317	
6	25			44.610	68.838	WH 5	mud, sand, gravelly		x	x	0.634	26.864	6.482	
6	25			44.596	68.824	WH 6	fine, medium sands		x	x	1.325	1.961	3.621	
6	25			44.602	68.824	WH 7	mud and organics	x	x		>4	70.373	21.842	
6	25			44.619	68.847	WH 8	medium, coarse sand		x	x	0.659	4.234	2.276	
6	25			44.613	68.851	WH 9	silty mud, sand	x	x		>4	79.635	20.553	
6	25			44.613	68.846	WH 10	coarse sand, cobbles		x	x	0.454	1.846	1.710	
6	25			44.607	68.845	WH 11	woodchips, mud	x	x		>4	77.303	23.640	
6	25			44.600	68.830	WH 12	woodchips		x				81.776	Predominantly organic matter
6	25			44.624	68.850	WH 13	fine, medium sand		x	x	1.163	2.307	2.903	
6	25			44.639	68.837	Winterport	coarse sand, gravel		x	x	<0	2.421	2.086	

Table 1. Grab sample analyses and characteristics for April, May, and June.

was performed on samples at each phi interval to avoid including organic material in grain size calculations. The median grain size of each sample was calculated based on cumulative frequency curves. For grabs with a median grain size coarser than 2 phi (0.25 mm), subsamples were re-sieved for 0, 1, 2, 3, and 4 phi (1, 0.5, 0.25, 0.125, 0.0625 mm, respectively) fractions and subsequent loss on ignition was performed to remove organics. For grabs with a median grain size finer than 4 phi (0.0625 mm), subsamples were processed with 30% hydrogen peroxide to remove organics. Samples were then sieved at 4 phi (0.0625 mm) and the fine percentages were processed by a Sedigraph 5120 (Micromeritics Instrument Corporation), which uses settling rates to determine particle size. June samples were used for these analyses.

Spatial Surveys

Shipboard surveys repeated over 12 hours were conducted during each field experiment to map flow conditions and water column structure throughout the estuary over a tidal cycle. A hand-deployable CTD (RBR Ltd.), optical backscatterance sensor (OBS; Campbell Scientific, Inc.), and bottom-tripped Niskin bottle were used to profile the water column and collect bottom water samples over four survey lines: Verona, Orland, Frankfort Flats, and a large-scale survey from Fort Point to Bangor (Figure 9). Surface water samples were also collected over these survey lines. During the June experiment, only the large scale, Frankfort Flats, and Orland surveys were conducted due to vessel troubles. There were 790 casts of this package and 68 water samples were collected over April, May, and June. Water samples were filtered with 0.45 µm filters, dried, and weighed to calculate suspended-sediment concentrations.

A RDI workhorse 1200 kHz acoustic Doppler current profiler (ADCP) was mounted to the side of the R/V *Mytilus* (Woods Hole Oceanographic Institution) over the Verona, Orland, and Frankfort Flats survey lines in April, May, and June. ADCP data were not collected over the large-scale survey lines. Velocity data were rotated to along- and across-channel using the direction of maximum variance. Acoustic backscatter intensity was used as a qualitative approximation of suspended-sediment concentration. More intense backscatter signals are indicative of higher suspended-sediment concentrations in the water column.

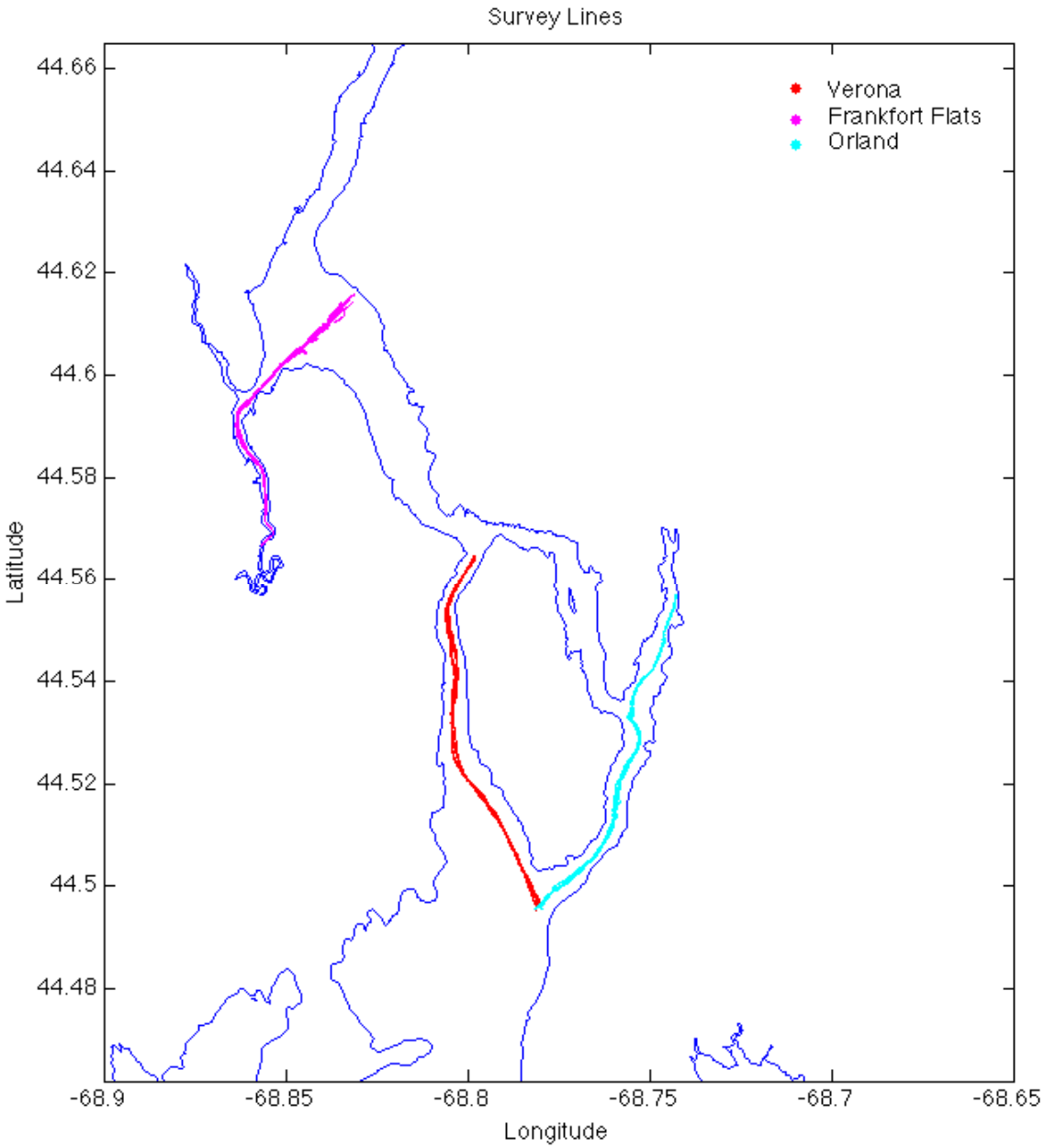

Figure 9. Spatial surveys were conducted in April, May, and June 2010 over four lines: Verona, Orland, Frankfort Flats, and a large-scale survey. The large-scale survey is not shown on this figure. Data from the Frankfort Flats survey line are presented in this paper.

Time Series Measurements

Surface moorings and bottom tripods were deployed April 2, 2010 and recovered June 27-29, 2010 at six locations in the lower Penobscot River Estuary to record temporal variability of water column structure and flow conditions (Figure 6). Tripods deployed at the deepest locations, Fort Point and Verona, had upward-looking 600 kHz ADCP, RBR CTD, OBS, and pressure gauges; tripods deployed at Winterport and Frankfort Flats had upward-looking 1200 kHz ADCP, RBR CTD, OBS, and pressure gauges; and tripods deployed at Mendall and Orland had upward-looking 1500 kHz Nortek Aquadops, RBR CTD, OBS, and pressure gauges. The Fort Point, Verona, and Winterport tripods were located within the thalweg. The Frankfort Flats tripod was located east of the thalweg, in shallower waters. Each tripod had an accompanying surface mooring with an RBR CTD to record surface salinity. Sampling intervals were between 5 and 30 minutes, but mooring and tripod data were re-sampled to 5 minutes to maintain resolution of the data. The along- and across-channel velocities were rotated in the same manner as velocities from the surveys. The tidal hour is referenced to low water at Portland, ME.

Results

The 2010 freshet peaked on April 1 with a magnitude of 1,876 m^3/s (Figure 7). The average freshet peak over the last 107 years of data recorded by the West Enfield U.S. Geological Survey site is 1,847 m^3/s, suggesting that the 2010 freshet was neither large nor small. The freshet in 2010 coincided with a spring tide.

During average conditions – low discharge, in between spring-neap tidal cycles – the tidal range of the Penobscot River Estuary is mesotidal, ~3.2 m. The tidal ranges at spring and neap tides are ~4.3 m and 2.4 m, respectively. The tidal ranges at Verona, a southern station, and Winterport, the northernmost station, are approximately equal (Figures 10, 11).

The side-scan mosaics reveal that the bed of the lower Penobscot River Estuary is dominated by bedforms, suggesting that sediment is coarse and transported as bedload. Fine sediments exist in patches, but are difficult to identify with certainty on side-scan mosaics (D.F. Belknap, pers. comm.).

The bed sediment characteristics are highly spatially variable (Figures 12-14, Table 1). Medium to coarse sand is the dominant grain size in the lower Penobscot River Estuary (Table 1). Grain-size distributions for southern and northern stations (Fort Point, Verona, and Winterport) are consistent from April to June, but results for stations between Verona and Frankfort Flats (Bridge Station, Bucksport, and Indian Point) are variable (Figures 12-14, Table 1). Median grain sizes for sediments collected at Indian Point, Bucksport, and Bridge Station vary between dominantly coarse (coarser than 4 phi, 0.0625 mm) and fine (finer than 4 phi, 0.0625 mm) over the study period. The sediments at the southern-most site, Fort Point, were consistently muddy. Sediments at the Verona site were consistently heterogeneous. Sediments collected at Frankfort Flats were consistently muddy. Sediments at the northern-most station, Winterport, were consistently coarse sand and fine gravel.

The extensive bottom-sediment survey conducted in June indicates that sediments in the channel of Marsh River are predominantly coarse sand to fine gravel (Figure 14, Table 1). The region of Frankfort Flats (24 to 20 km; Figure 8) has sediments that are dominantly coarse. However, a patch of fine sediments, including sites WH 9, Frankfort

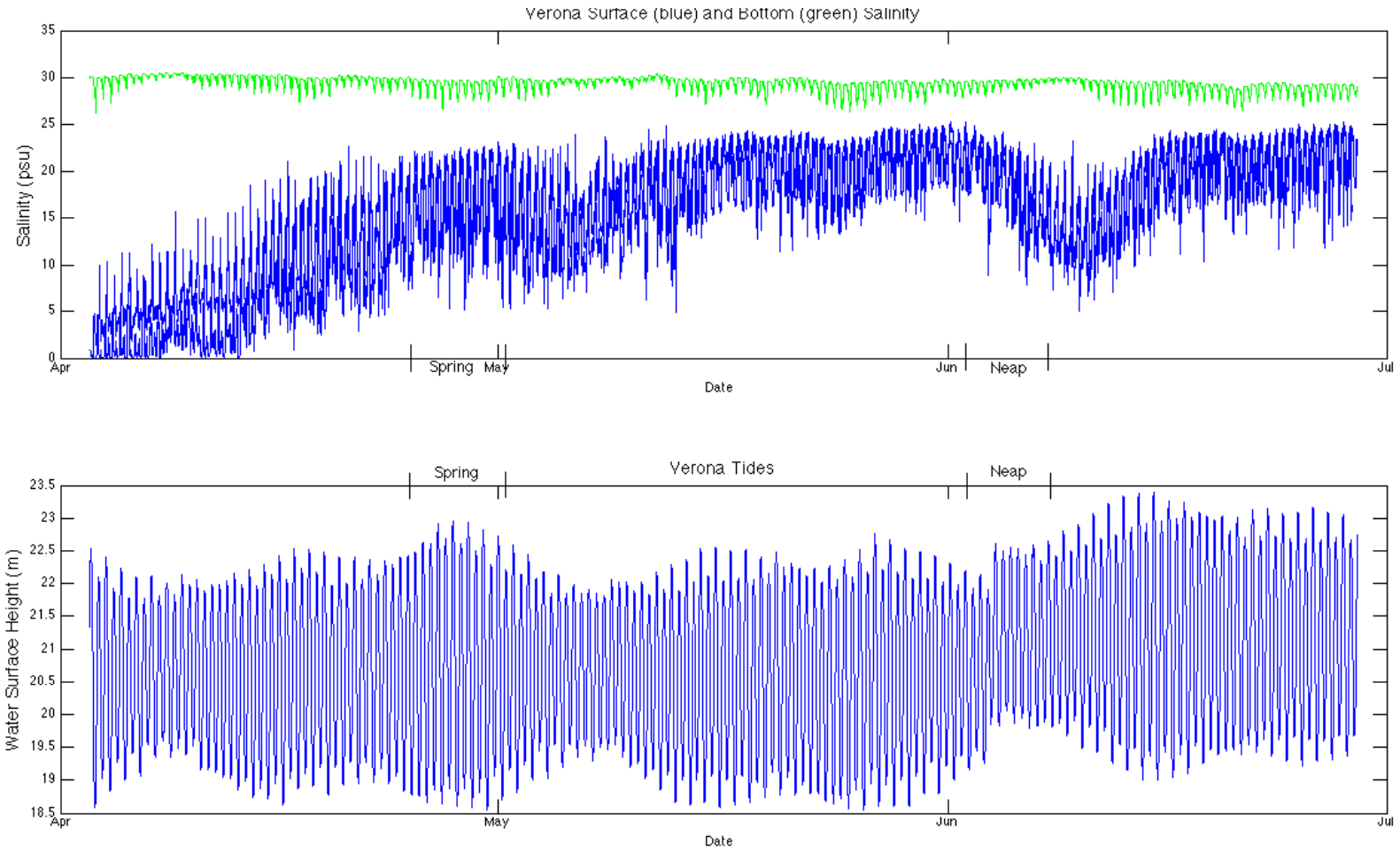

Figure 10. The top figure displays surface salinity in blue and bottom salinity in green from the Verona mooring and tripod from April through June. The bottom figure shows the water surface height in meters, which is indicative of the

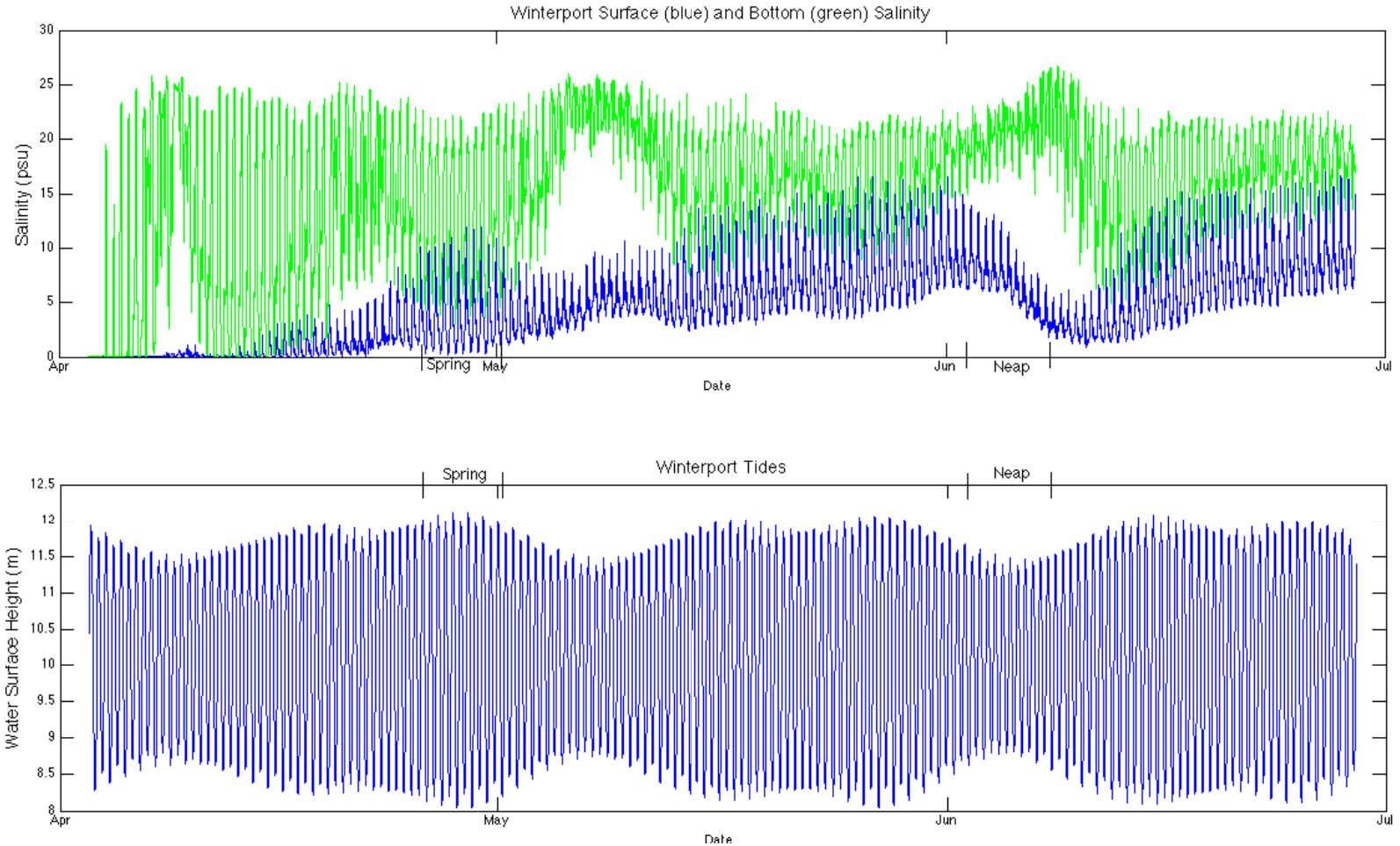

Figure 11. The top figure displays surface salinity in blue and bottom salinity in green from the Winterport mooring and tripod from April through June. The bottom figure shows the water surface height in meters, which is indicative of the

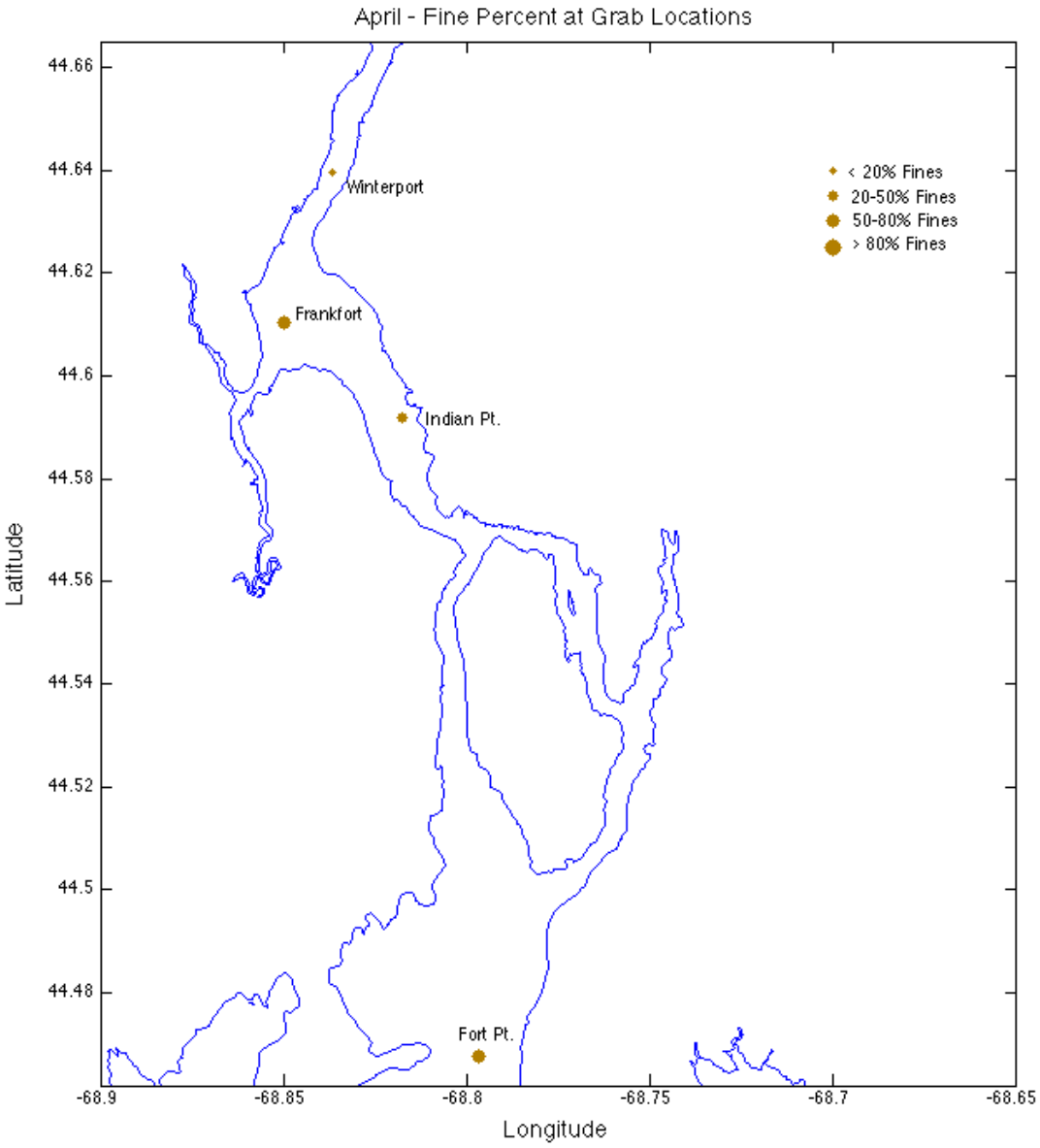

Figure 12. Grain size analysis results for April grab stations. 'Fine' is defined as finer than 0.0625 mm.

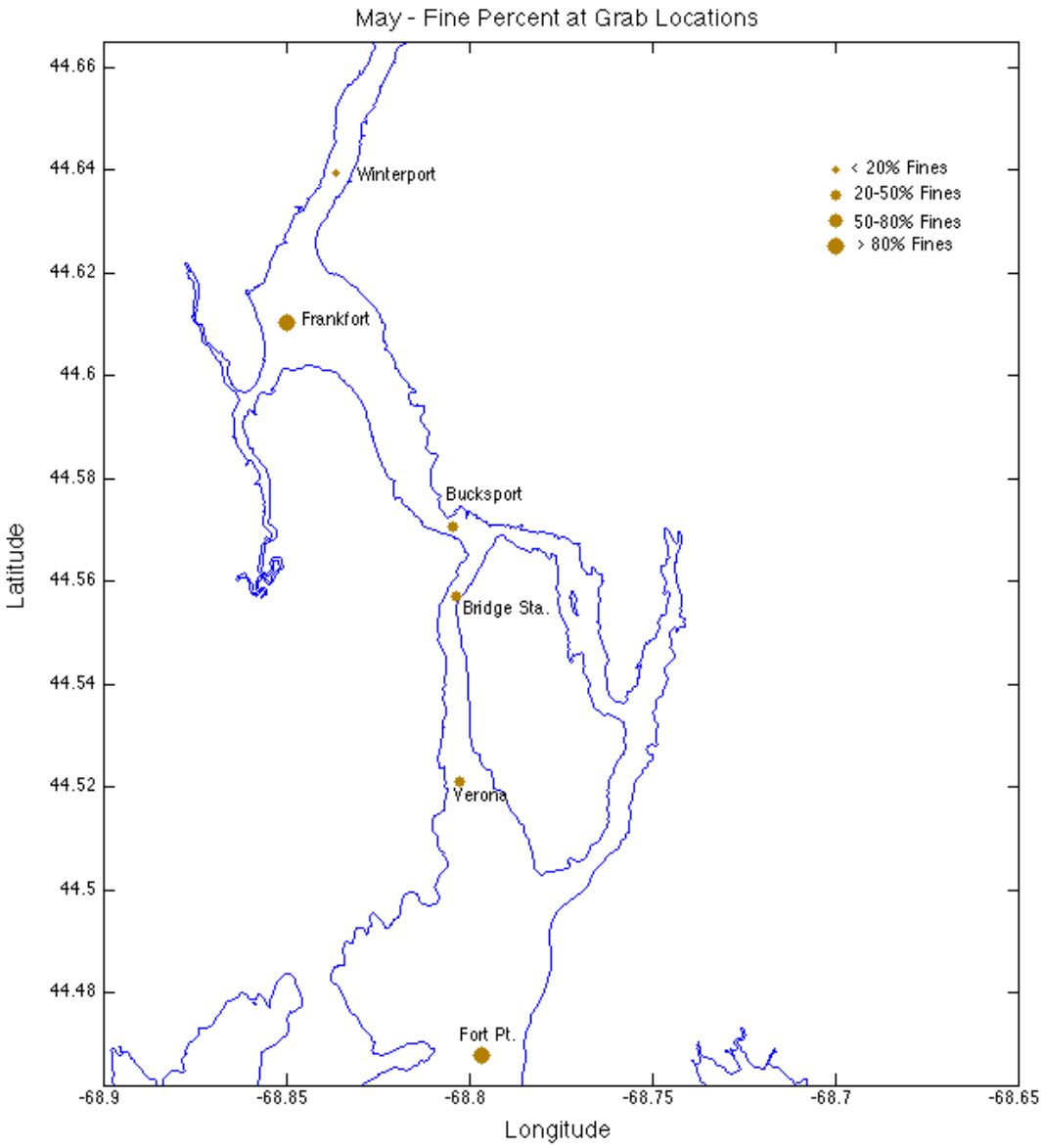

Figure 13. Grain size analysis results for May grab stations. 'Fine' is defined as finer than 0.0625 mm.

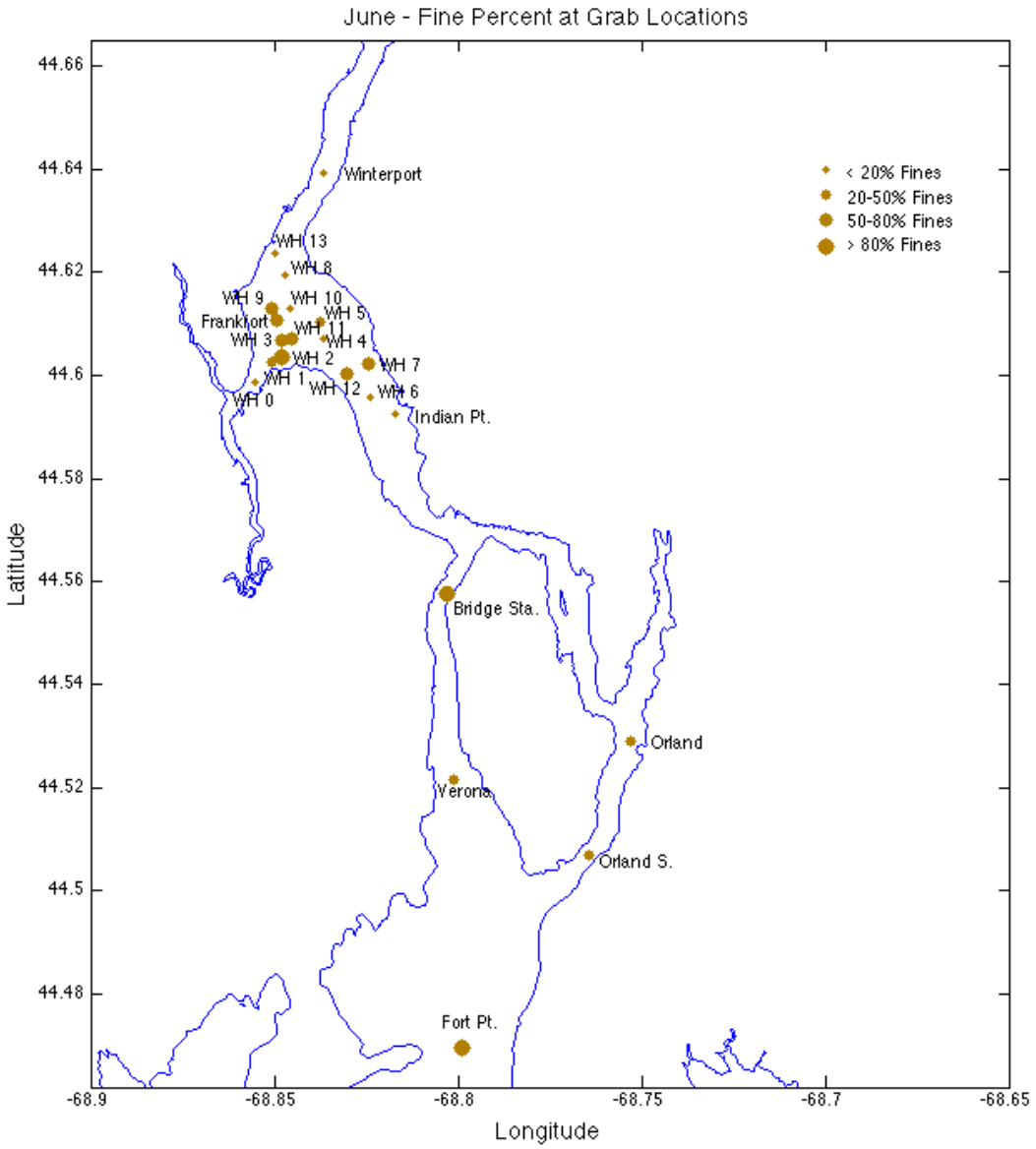

Figure 14. Grain size analysis results for June grab stations. 'Fine' is defined as finer than 0.0625 mm.

Flats, WH 3, and WH 11, exists in the thalweg of the Frankfort Flats reach (Figures 8, 15).

Maximum velocities along the Frankfort Flats survey line occur during maximum ebb. During the freshet, maximum ebb velocities in the thalweg were ~1.2 m/s and flood velocities were one-half the magnitude (Appendix: Figure A1). As discharge decreases, maximum flood and ebb velocities in the thalweg approached equivalence (Appendix: Figures A1-3b). Acoustic backscatter measured by the ADCP was converted to suspended-sediment concentration (mg/L) using an empirical equation determined from a calibration using collected water samples and OBS data. This equation is defined as:

$$Concentration = 1.6 * 5 * 10^{(0.045*(1.5*(amp-43)+0.55*20*log10(z)+1*0.5*z))} \quad (6)$$

where amp is the acoustic backscatter intensity and z is distance from the ADCP transducer (W.R. Geyer, pers. comm.). Maximum suspended-sediment concentrations were observed in the thalweg of the Frankfort Flats reach during flood currents (Figures 16, 17).

There is a prevalent across-channel flow during maximum flood and ebb currents in the thalweg at the Frankfort Flats survey line. The magnitude and direction of this flow at the bottom are ~0.2 m/s to the left during flood currents (Figures 16, 17) and ~0.2 m/s to the right during ebb currents (Figures 18, 19). There is also a weak surface flow in the opposite direction (Figures 16-19).

The large-scale salinity surveys conducted in April, May, and June indicate a landward migration of the salt intrusion as discharge decreases after the freshet (Figure 20). In April, the salt wedge extends only as far as kilometer 30, near Winterport, during high discharge and a spring tide (Figure 20). In June, low discharge and a spring tide promote mixing, as well as intrusion of the salt wedge to kilometer 42 (Figure 20). Fluctuations in stratification at the Verona and Winterport tripods are associated with spring-neap cycles, which may control the position of the salt wedge (Figures 10, 11).

At the Verona site, maximum suspended-sediment concentrations occur during the late ebb and early flood phase (Figure 21). However, at Winterport, maximum suspended-sediment concentrations occur during the late flood phase (Figure 22),

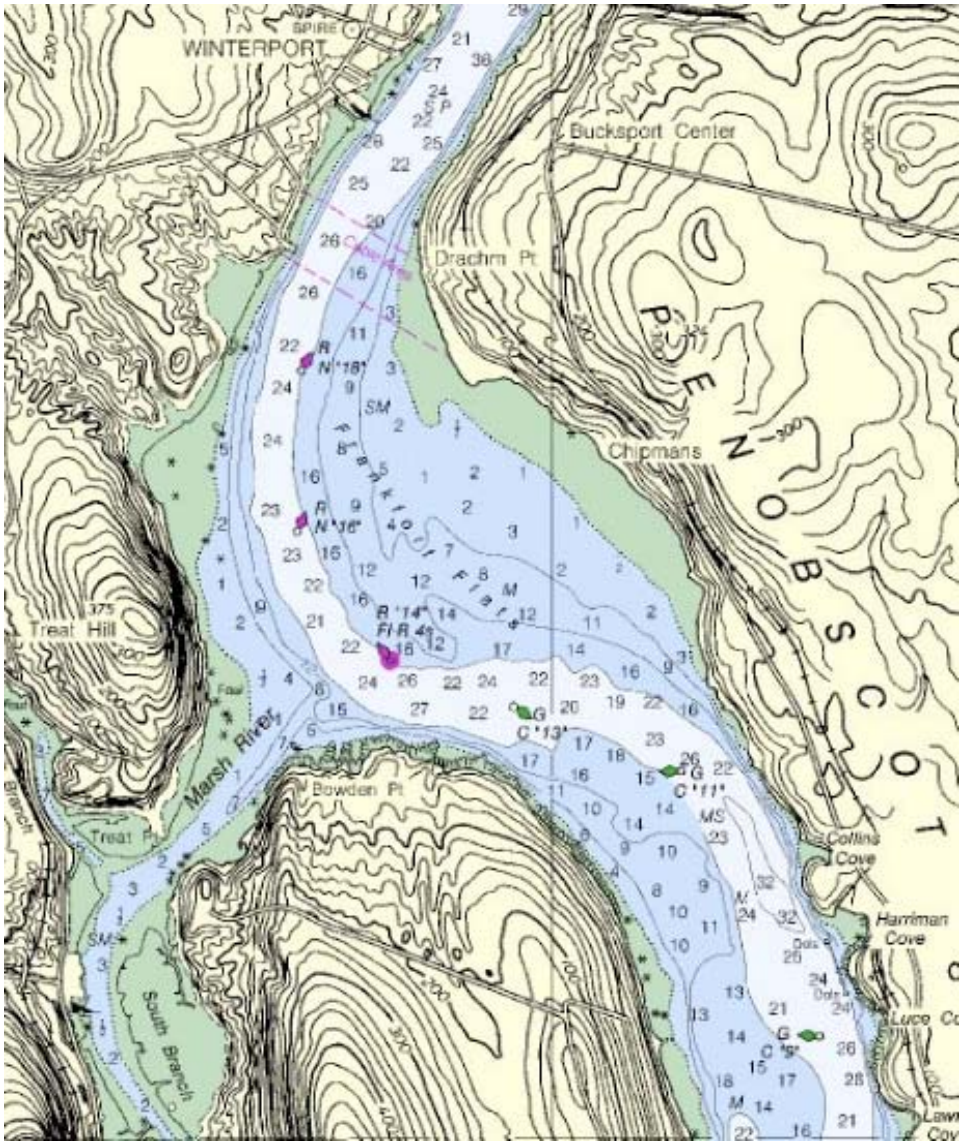

Figure 15. Bathymetry of the Frankfort Flats reach of the lower Penobscot River Estuary. Note that the channel meanders around a right-hand bend and a left-hand bend in this reach going upstream. (U.S. Geological Survey)

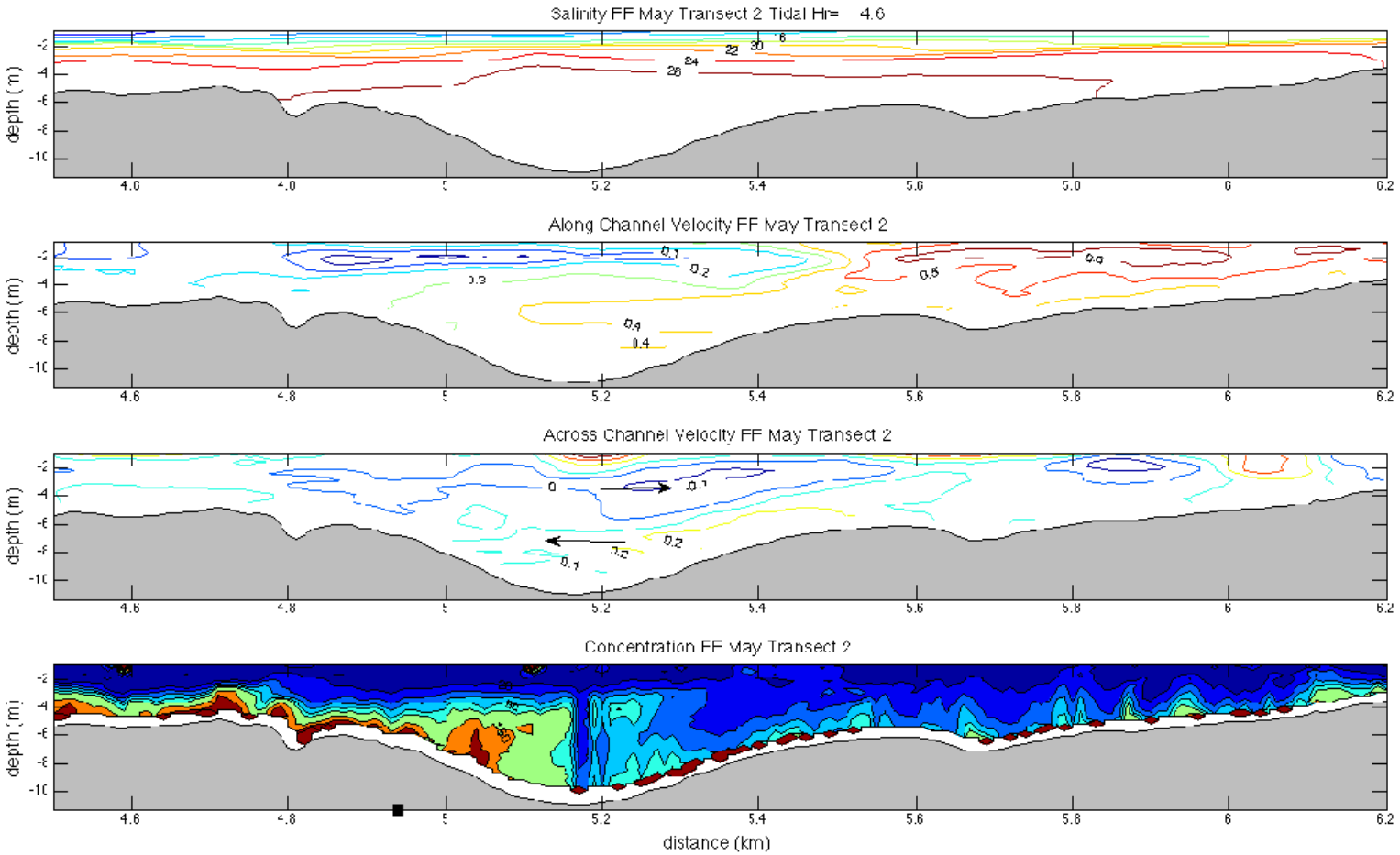

Figure 16. The salinity structure (psu), along-channel velocity (m/s), across-channel velocity (m/s), and suspended-sediment concentration (mg/L) during maximum flood in May along the Frankfort Flats survey line (Figure 9). For along-channel, positive velocities indicate flooding and negative velocities indicate ebbing. For across-channel, positive velocities indicate flow to the left and negative velocities indicate flow to the right, also indicated by the arrows. The black square marks the location of station WH 2.

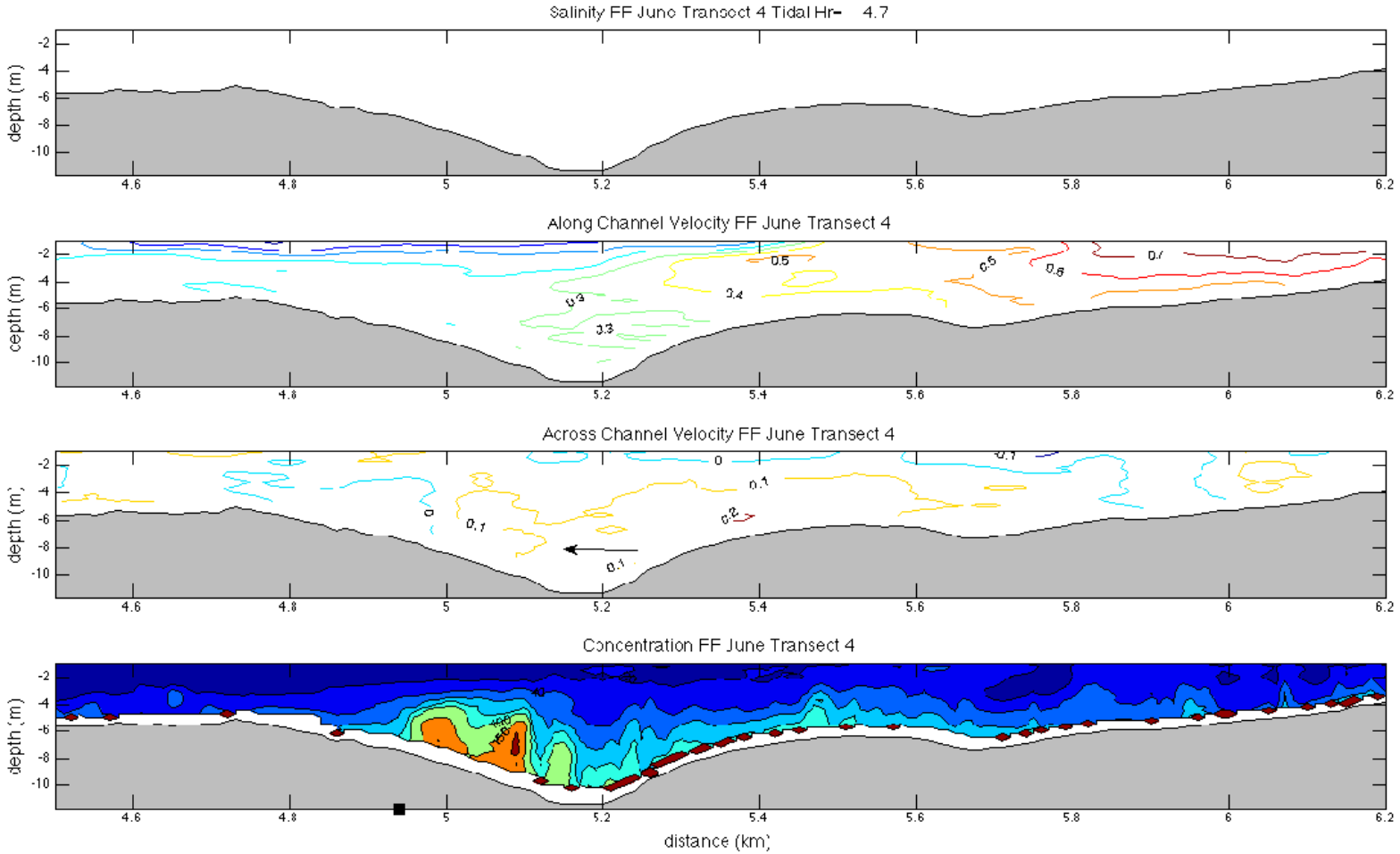

Figure 17. The salinity structure (psu), along-channel velocity (m/s), across-channel velocity (m/s), and suspended-sediment concentration (mg/L) during maximum flood in June along the Frankfort Flats survey line (Figure 9). For along-channel, positive velocities indicate flooding and negative velocities indicate ebbing. For across-channel, positive velocities indicate flow to the left and negative velocities indicate flow to the right, also indicated by the arrows. The black square marks the location of station WH 2.

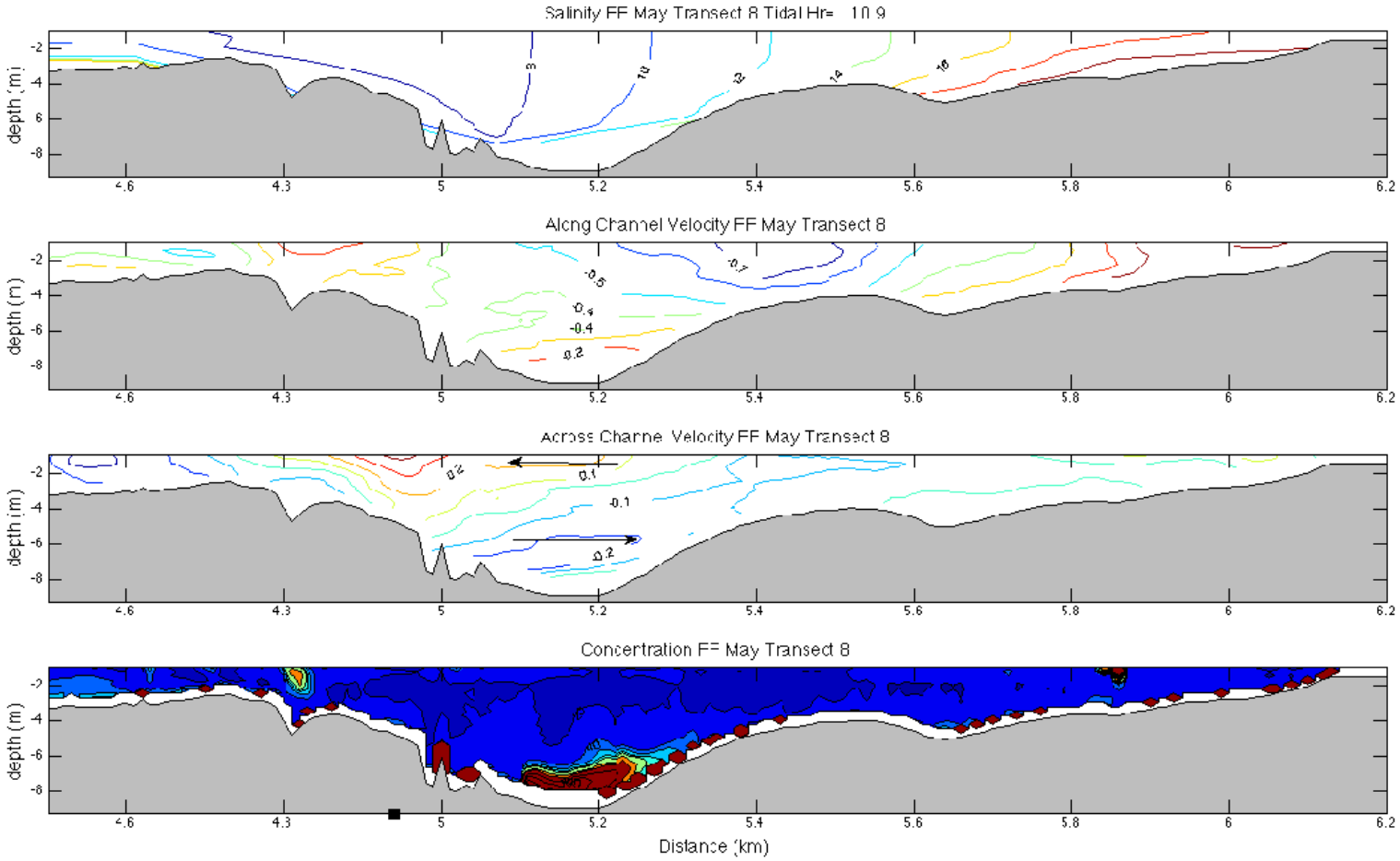

Figure 18. The salinity structure (psu), along-channel velocity (m/s), across-channel velocity (m/s), and suspended-sediment concentration (mg/L) during maximum ebb in May along the Frankfort Flats survey line (Figure 9). For along-channel, positive velocities indicate flooding and negative velocities indicate ebbing. For across-channel, positive velocities indicate flow to the left and negative velocities indicate flow to the right, also indicated by the arrows. The black square marks the location of station WH 2.

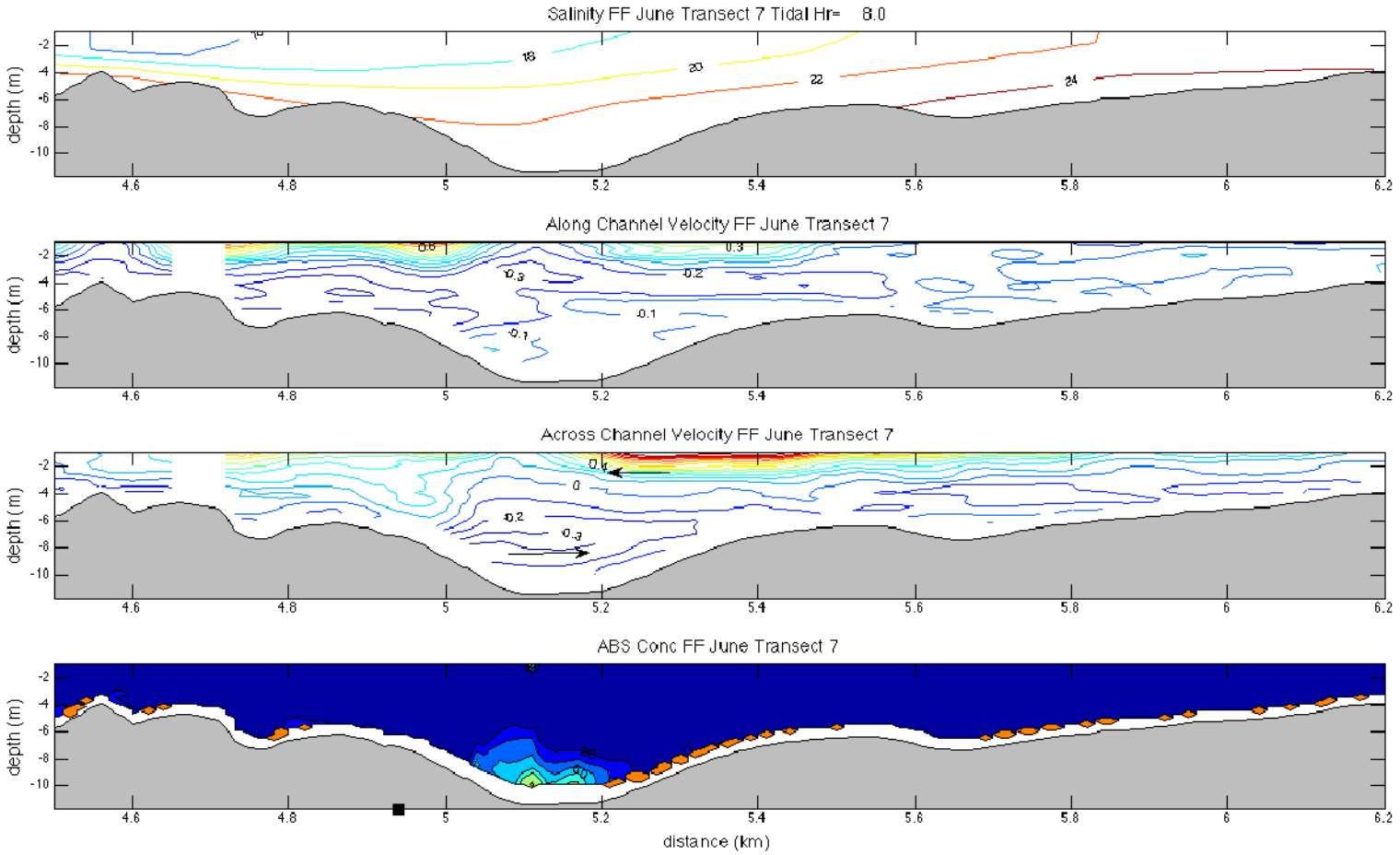

Figure 19. The salinity structure (psu), along-channel velocity (m/s), across-channel velocity (m/s), and suspended-sediment concentration (mg/L) during maximum ebb in June along the Frankfort Flats survey line (Figure 9). For along-channel, positive velocities indicate flooding and negative velocities indicate ebbing. For across-channel, positive velocities indicate flow to the left and negative velocities indicate flow to the right, also indicated by the arrows. The black square marks the location of station WH 2.

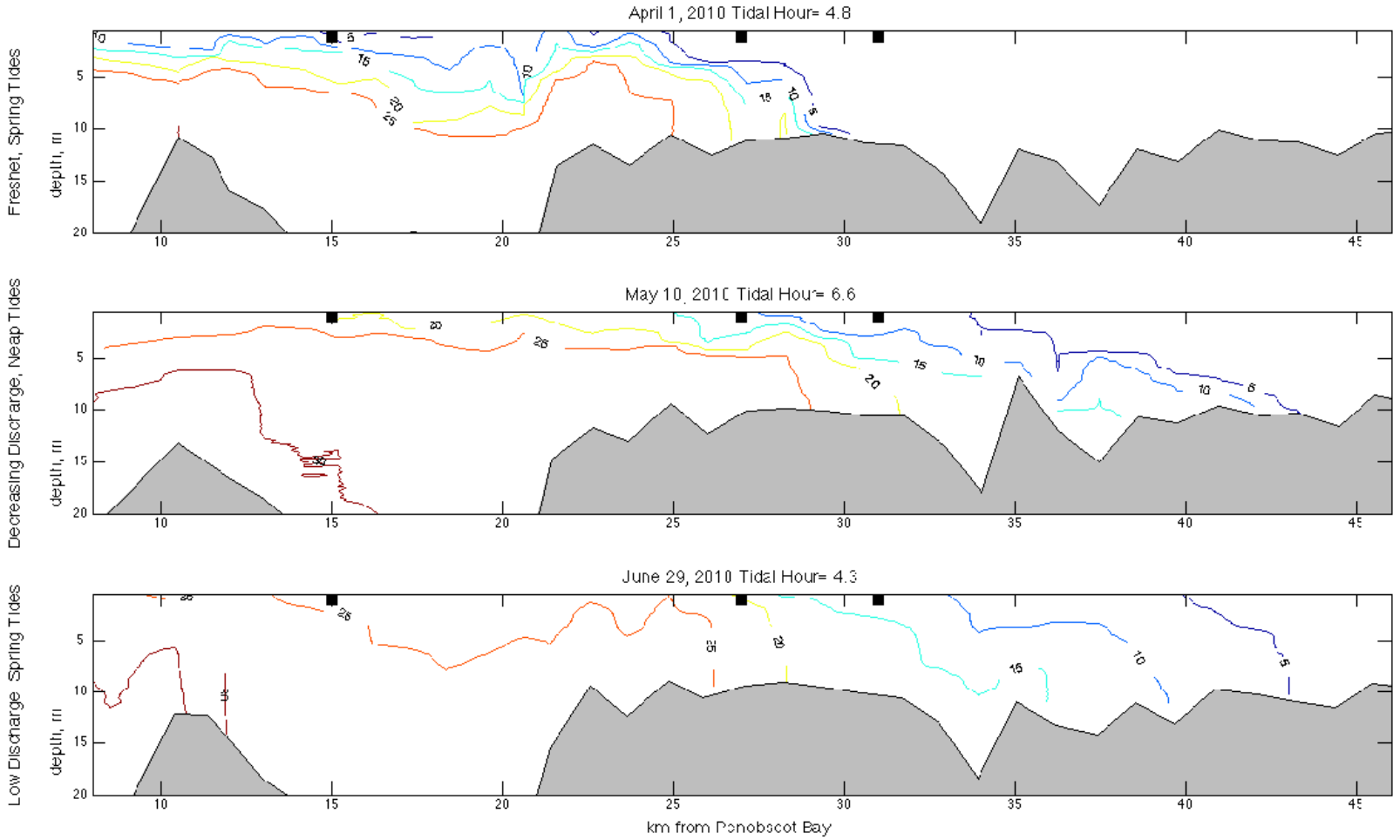

Figure 20. Salinity structure in April, May, and June, showing the landward progression of the salt wedge after being pushed seaward during the April freshet. The black squares are kilometers ~15, 27 and 31 are the Verona, Frankfort Flats, and Winterport stations, respectively.

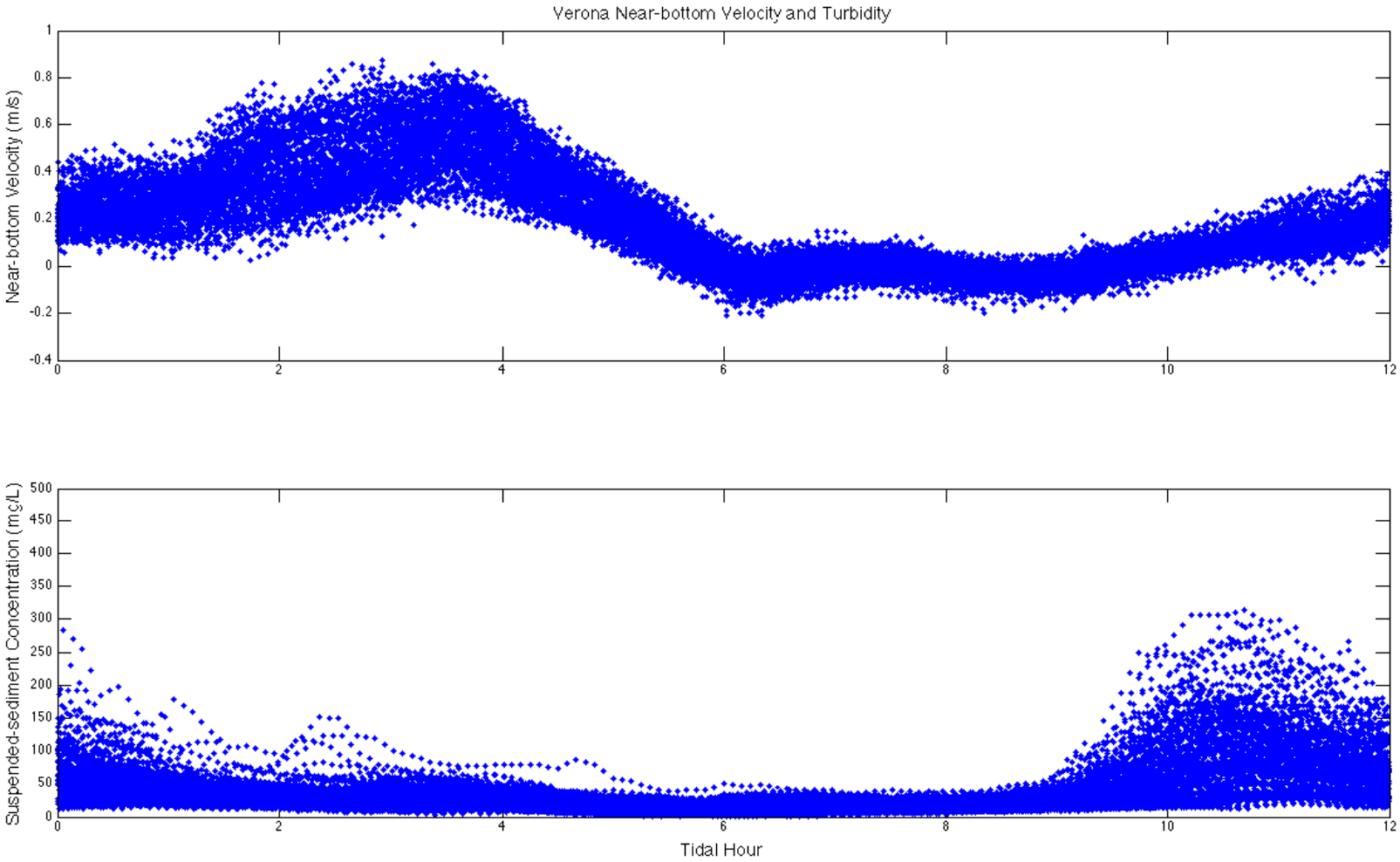

Figure 21. The near-bottom velocity at the Verona tripod as referenced to the tidal hour (a). Suspended-sediment concentration at the Verona tripod as referenced to the tidal hour (b). Maximum turbidity occurs during late ebb. Tidal Hour 0 is low water at Portland, ME.

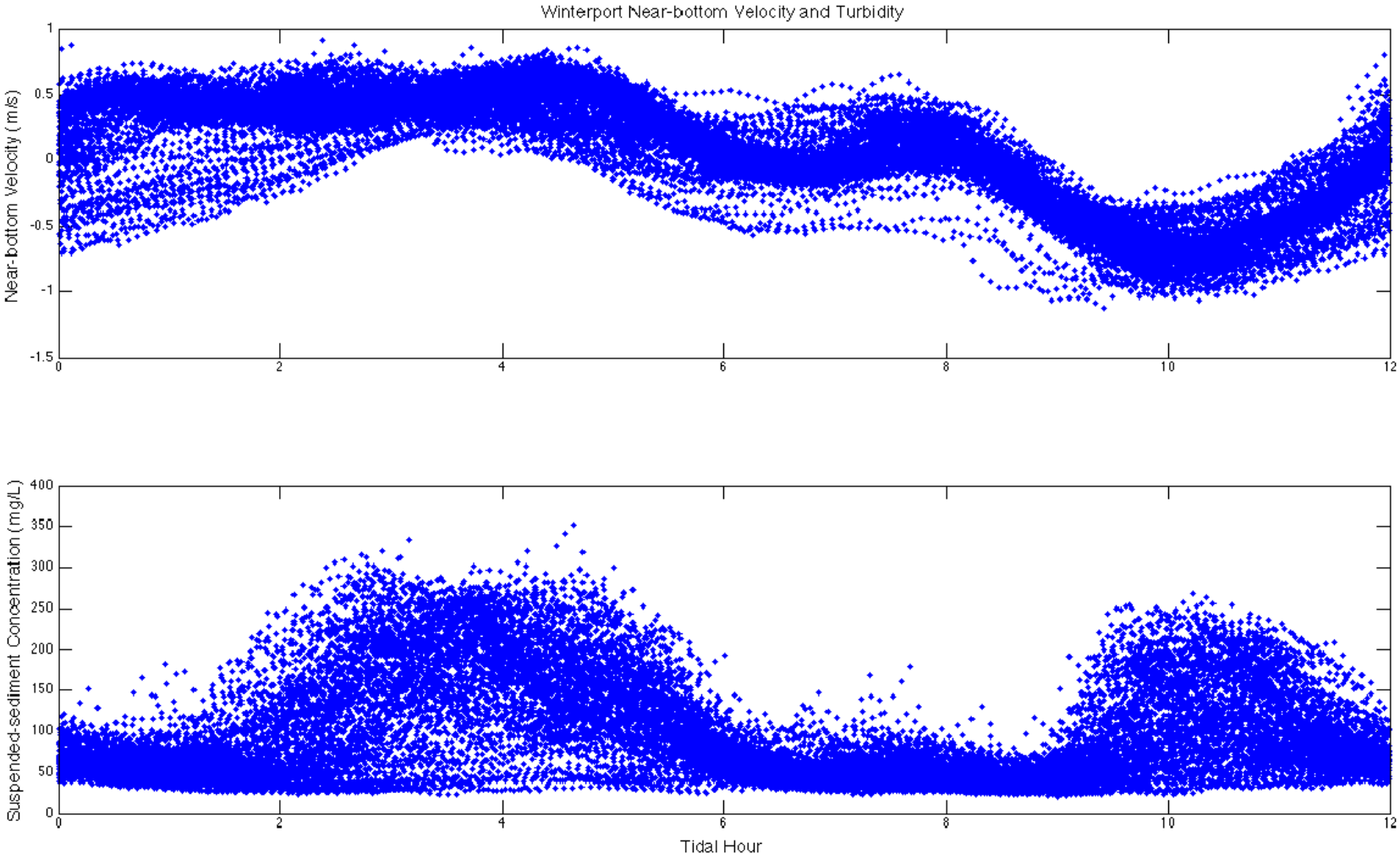

Figure 22. The near-bottom velocity at the Winterport tripod as referenced to the tidal hour (a). Suspended-sediment concentration at the Winterport tripod as referenced to the tidal hour (b). Maximum turbidity occurs during late ebb. Tidal Hour 0 is low water at Portland, ME.

suggesting that there is a source of sediment between these two stations. Maximum suspended-sediment concentration variability over longer timescales is associated with spring-neap cycles (Figure 23).

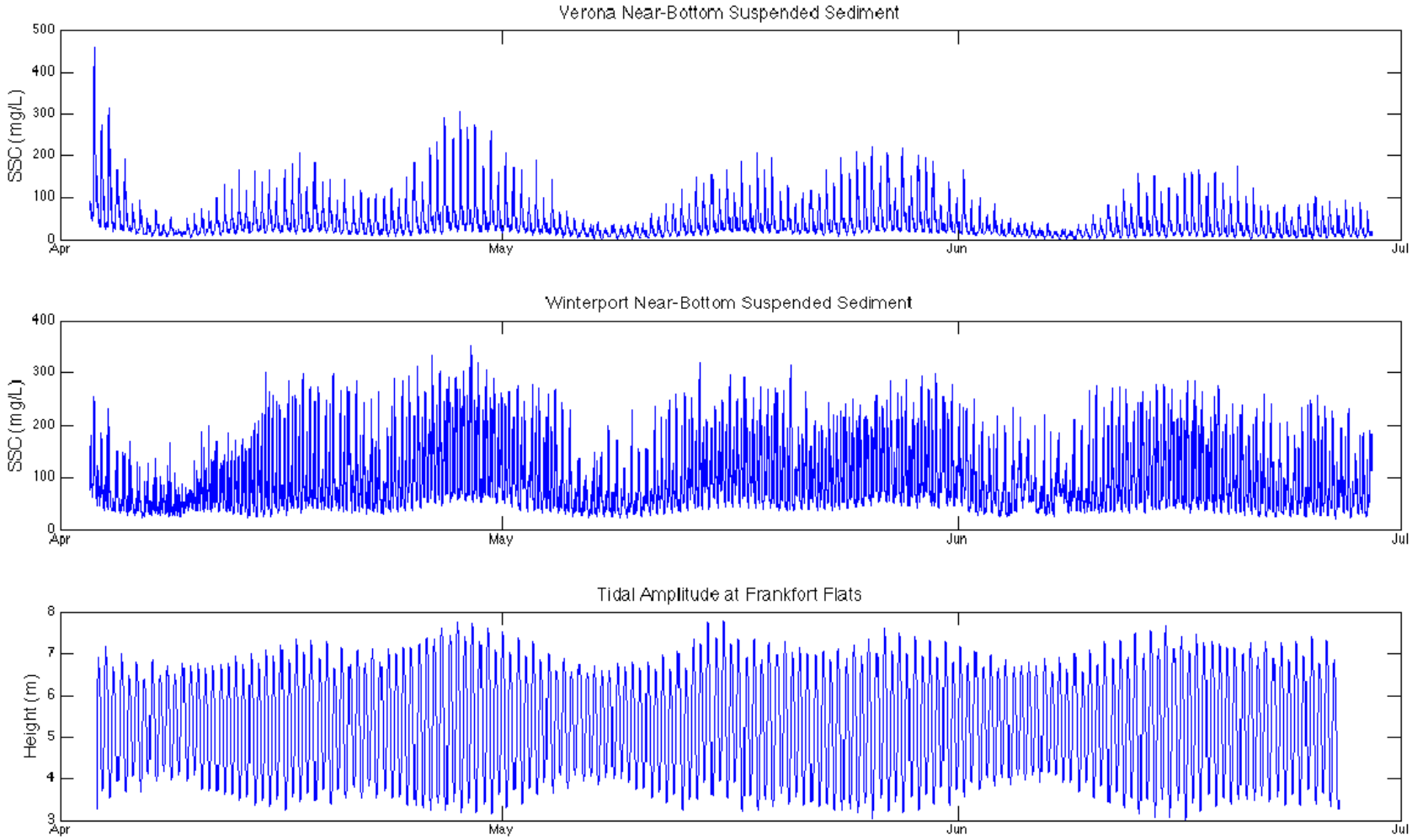

Figure 23. Near-bottom suspended-sediment concentrations at the Verona and Winterport tripods and the tidal amplitude at Frankfort Flats to show correlations in resuspension and the spring-neap and daily tidal cycles.

Discussion

The purpose of this study was to characterize the bed sediments and determine the mechanisms for fine-sediment transport and deposition in the lower Penobscot River Estuary. To summarize the results, fine sediments are located in a patch within the Frankfort Flats reach at sites WH 9, WH 3, WH 11, and Frankfort Flats (Figure 14, Table 1). Coarse sediments are located at Winterport, sites within Marsh River, and other sites within the Frankfort Flats reach (Figure 14, Table 1). Sediments are variable at Bridge Station, Bucksport, and Indian Point over April, May, and June, but the southernmost and northernmost stations (Fort Point, Verona, and Winterport) are consistent (Figures 12-14, Table 1). This distribution is likely created by tidal flow conditions, the location and migration of the salt wedge, and lateral circulation.

Potential for Resuspension

The Frankfort Flats reach is of interest because it contains a patch of fine sediments bounded on both sides by coarse sediments. Critical shear stress for the median grain size of sediment at sites within the Frankfort Flats reach was compared to maximum stress determined from tidal flow conditions to determine if bed sediments reflect the energy of the flow environment, or are lag deposits from prior stronger flow conditions. Bottom sediment samples collected over the Frankfort Flats survey line include sites WH 0, WH 1, WH 2, and WH 5 (Figure 24).

The shear stress provided by the flow was calculated using the Quadratic Stress Law (Equation 4), where C_{100} = 3.0 x 10^{-3} and ρ = 1000 kg/m^3 (Sternberg, 1972). Maximum velocity at one meter above the bed (u_{100}) occurs at WH 1 during late ebb currents (tidal hour 11.0) and is 0.36 m/s (Appendix: Figures A4a, A4b). The maximum shear stress provided by the flow at site WH 1 throughout the tidal cycle is 0.40 Pa (kg/ms^2). The median grain size of bottom sediments at site WH 1, located in the channel of Marsh River, is 2.92 phi (0.132 mm) (Figure 24, Table 1). The critical shear stress for the median grain size at site WH 1 was determined using the Shield's Diagram (Middleton and Southard, 1984) and is 0.15 Pa. $u_{100}|u_{100}|$ is proportional to the shear stress and, therefore, easy comparisons of observed and critical shear stresses were made. The critical shear stress of sediments from site WH 1 is exceeded for ~3.25 hours around maximum flood and ~3.55 hours around maximum ebb (Figure 25).

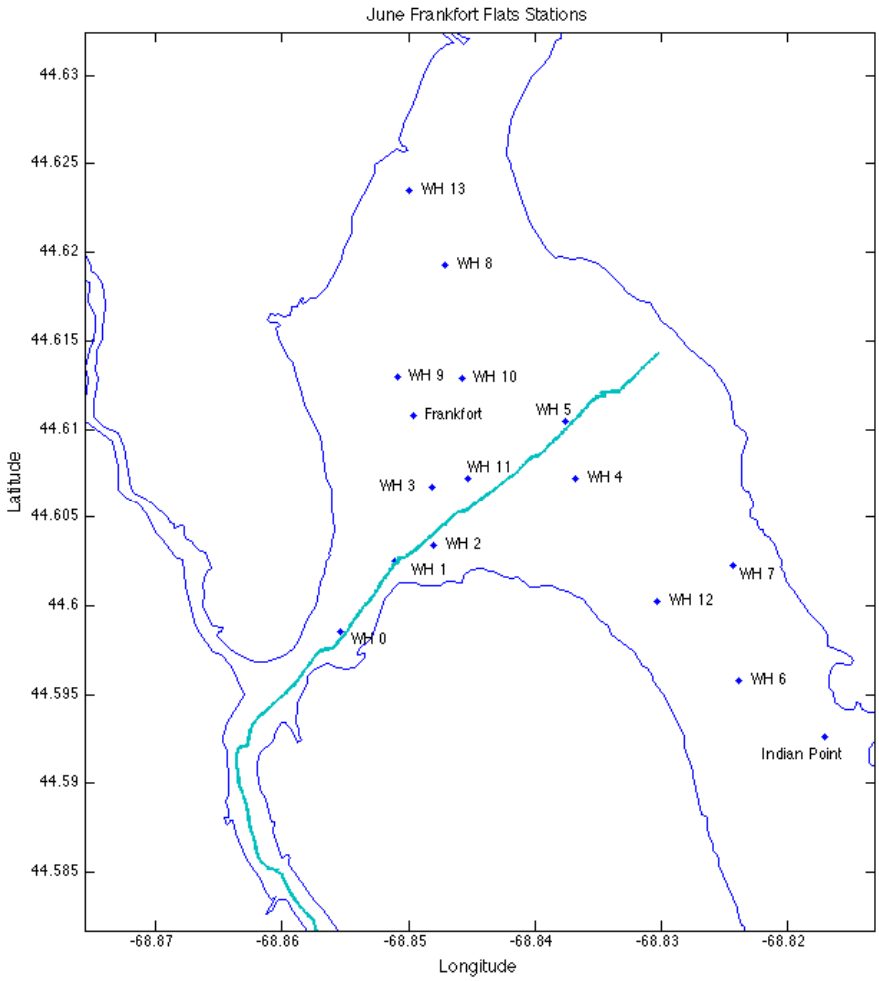

Figure 24. Grab sampling locations in the Frankfort Flats reach of the Penobscot River Estuary in June. The ADCP and CTD Frankfort Flats survey line is superimposed on the grab locations. The median grain sizes of sediments collected at sites WH 0, WH 1, and WH 5 were used to compare the shear stress provided by the flow at the sites and the critical shear stress of the sediments to determine if sediments are transported by tidal currents or are lag deposits.

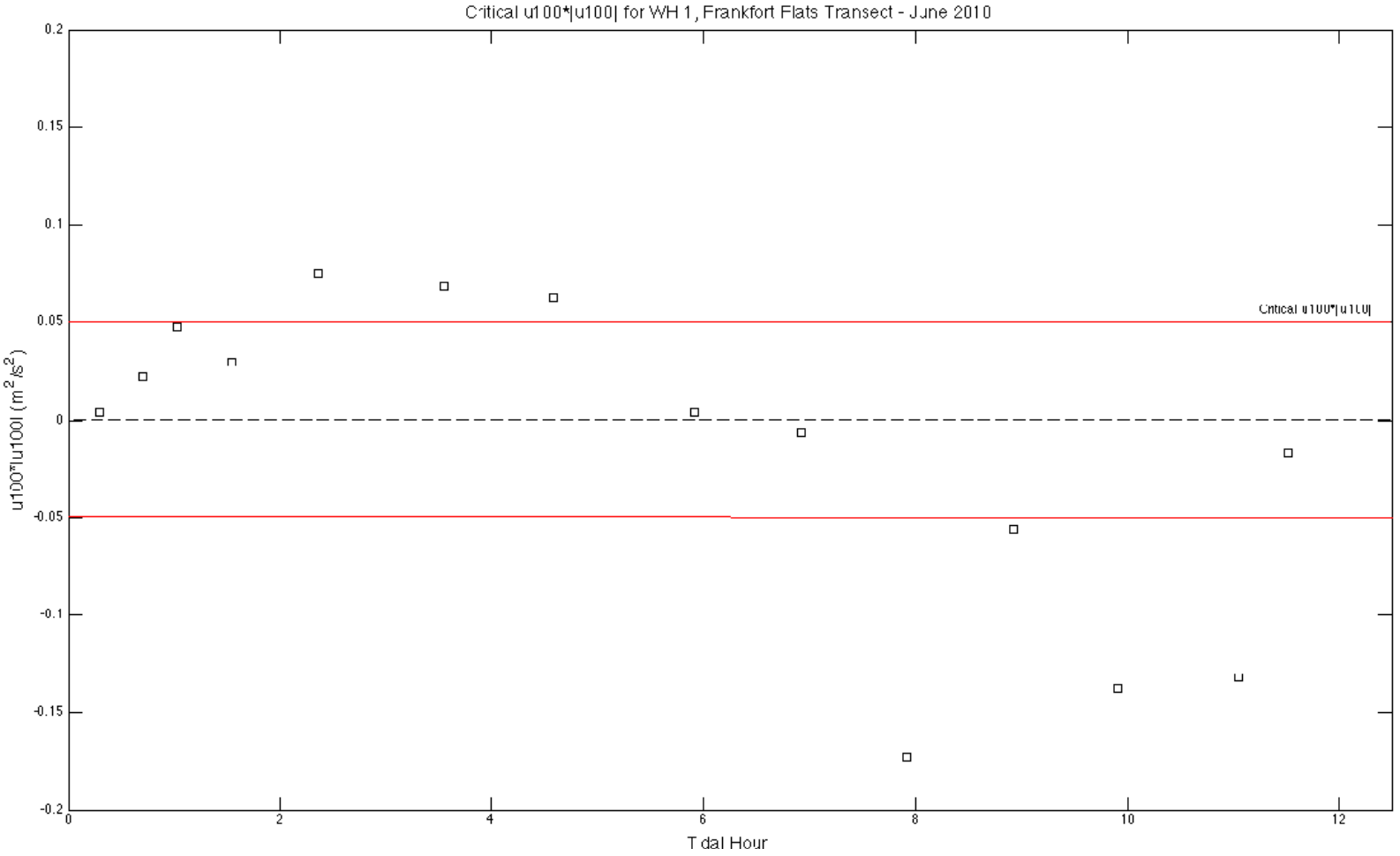

Figure 25. Excess u100*|u100| throughout the tidal cycle with reference to the critical u100*|u100| for the median grain size of sediment at WH 1.

Similar calculations were performed for sediments from sites WH 0 and WH 5, using median grain sizes of 0 phi (1 mm) and 0.63 phi (0.646 mm), respectively (Table 1). Although the median grain size of sediment from site WH 0 is coarser than 0 phi, grain size data were not collected coarser than 0 phi. Approximately 70% of sediment from site WH 0 is coarser than 0 phi; therefore, critical shear stress calculated from this grain size represents the minimum shear stress needed to resuspended 30% of sediment at this location (Table 1). Maximum velocity at one meter above the bed at site WH 0 occurs during flood currents (tidal hour 3.6) and is 0.40 m/s (Appendix: Figures A5a, A5b). The maximum shear stress provided by the flow is 0.49 Pa. The critical shear stress for this sediment is 1.60 Pa. Using $u_{100}|u_{100}|$ it is shown that the critical shear stress is not exceeded throughout the tidal cycle (Figure 26). The median grain size of sediment at site WH 5 is 0.63 phi (0.646 mm) and maximum velocity at one meter above the bed occurs during late flood (tidal hour 4.4) with a magnitude of 0.51 m/s (Appendix A: Figures A6a, A6b). The maximum shear stress provided by the flow is 0.79 Pa. The critical shear stress for this sediment is 0.32 Pa. The critical shear stress is exceeded for ~3.00 hours around maximum flood currents, but is not exceeded during ebb currents (Figure 27). A summary of these calculations can be found in the following table:

Table 2. The potential for resuspension of sediment at locations WH 1, WH 0, and WH 5 along the Frankfort Flats survey line (Figure 24) as determined by flow conditions and the median grain size (Table 1).

Location	u_{100}(m/s)	Max τ_0 (Pa)	D_{50} (phi)	D_{50} (mm)	Critical τ_0 (Pa)
WH 1	0.36	0.40	2.92	0.132	0.15
WH 0	0.40	0.49	0	1	1.60
WH 5	0.51	0.79	0.63	0.646	0.32

Sediment at sites WH 1 and WH 5 can be transported as bedload during certain phases of the tidal cycle based on the comparison of critical shear stress of bed sediments and the maximum shear stress provided by the flow. Sediment at site WH 0 is likely a lag deposit because the maximum shear stress provided by the flow does not exceed the critical shear stress of the bed sediment throughout the tidal cycle. Velocities in the Frankfort Flats reach of the Penobscot River Estuary are capable of transporting medium

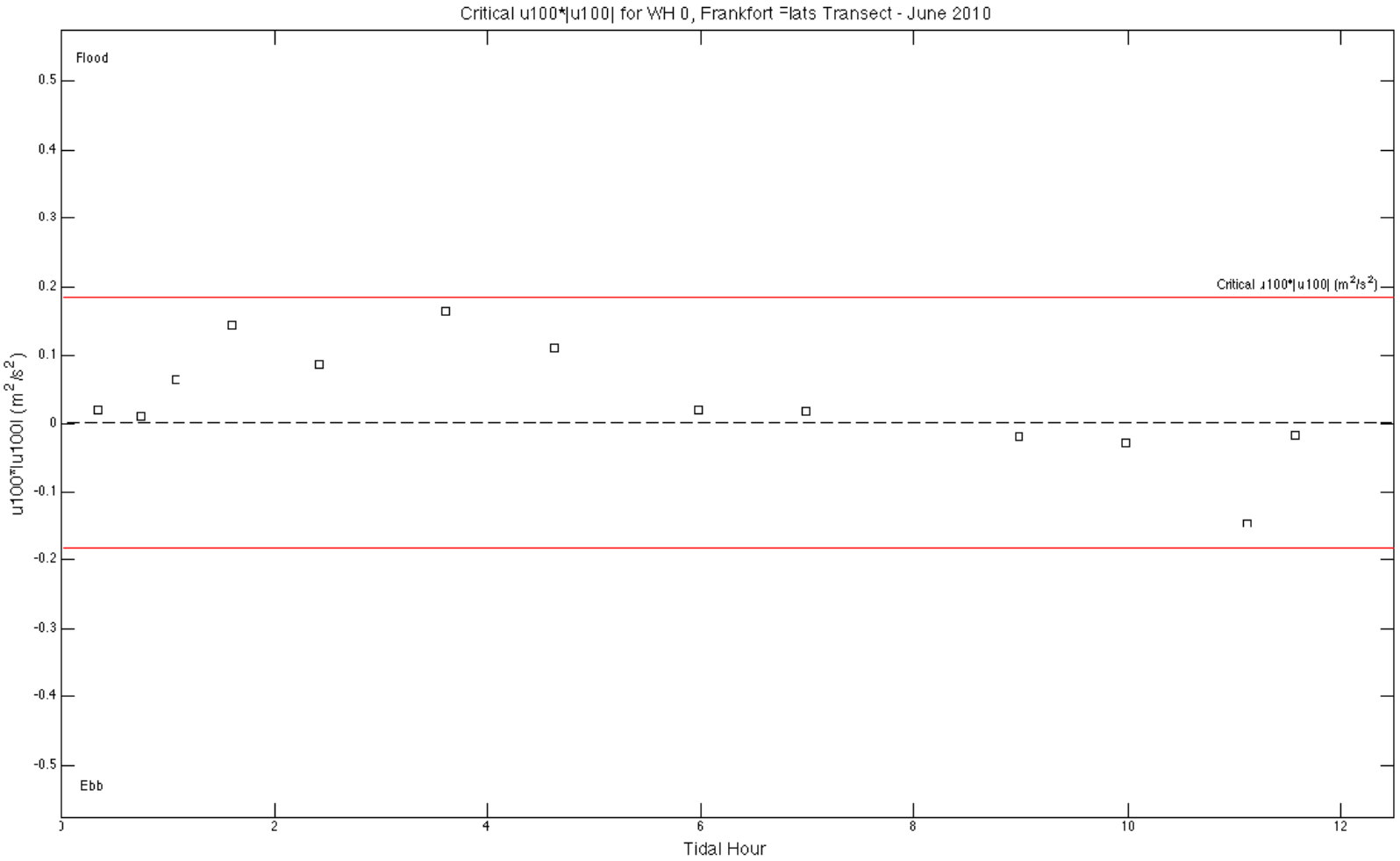

Figure 26. Excess u100*|u100| throughout the tidal cycle with reference to the critical u100*|u100| for the median grain size of sediment at WH 0.

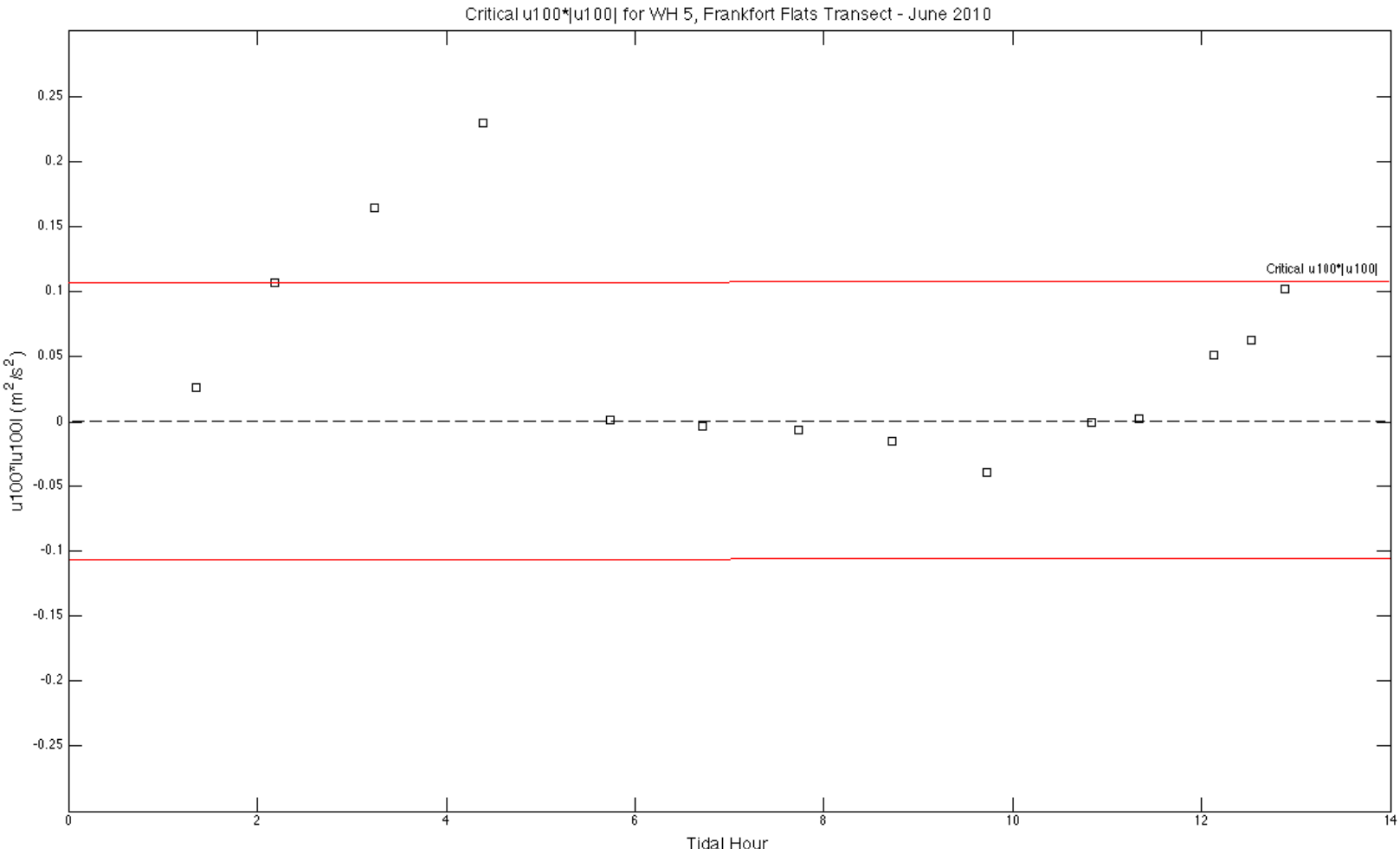

Figure 27. Excess u100*|u100| throughout the tidal cycle with reference to the critical u100*|u100| for the median grain size of sediment at WH 5.

to coarse sands, as suggested by the predominance of this size sediment throughout the estuary and specifically in this reach. The presence of fine sediment in the thalweg of the Frankfort Flats reach, where velocities are expected to be highest, cannot be explained by the local variations in shear stress. An alternative explanation that will be explored below is that there may be a trapping mechanism present at this location. Without a trapping mechanism, bottom sediments in this reach would be stripped of all fine sediments, which would be transported in suspension.

The Salt Wedge

The turbidity maximum is a region of high suspended-sediment concentrations, usually located near the landward extent of the salt intrusion. The salinity structure of the estuary during April, May, and June indicates a landward progression of the salt intrusion (Figure 20). ADCP data were not collected during the large-scale surveys, and the Frankfort Flats tripod and mooring was not located in the thalweg, thus the existence and location of a turbidity maximum based on direct observations of suspended-sediment concentrations cannot be confirmed. However, maximum near-bottom suspended-sediment concentrations at Verona occur during late ebb and very early flood currents (tidal hour ~10.5), suggesting that suspended sediment is coming from a source upstream of the Verona site and that both resuspension and advection are responsible for suspended-sediment distributions (Figure 21). Maximum suspended-sediment concentrations at Winterport occur during mid to late flood currents (tidal hour ~4), suggesting that suspended sediment is coming from a source downstream of this location (Figure 22). The timing of maximum turbidity and the large-scale salinity structure indicate that a turbidity maximum likely exists in the thalweg at the Frankfort Flats reach of the lower estuary. This is consistent with the deposit of fine sediments in the thalweg at this reach (Figure 14).

Seasonal Variations in the Salt Wedge

The location of the landward extent of the salinity intrusion, likely accompanied by high suspended-sediment concentrations, is dependent on the interaction of discharge, daily tidal currents, and spring-neap cycles. During the 2010 freshet, at times of maximum flood currents during spring tides, the landward extent of the salt intrusion was located between 25 and 30 km from Penobscot Bay (Figure 20). Frankfort Flats is ~27

km from Penobscot Bay. The combination of ebb currents, high discharge, and resuspension during spring tides likely pushes the salt wedge downstream, although there are no direct observations because tripods were too far south and north of the likely locations of the turbidity maximum (Frankfort Flats reach). The consistency of the coarse median grain size of sediments collected at the Verona site in April, May, and June suggests that the turbidity maximum is not pushed as far seaward as the Verona station (Figures 12-14, Table 1). The water column at Verona is consistently highly stratified over the study period (Figure 10), further suggesting that the turbidity maximum is not pushed as far seaward as this location. Similarly, the consistency of the coarse median grain size of sediments collected at the Winterport site in April, May, and June suggests that the turbidity maximum does not migrate landward to Winterport (Figures 12-14, Table 1).

The variability in bottom-sediment characteristics at Bridge Station, Bucksport, and Indian Point sampling sites observed in April, May, and June, (Figures 12-14, Table 1), indicate an upstream migration of the turbidity maximum, consistent with the upstream progression of the salt intrusion (Figure 20). Bottom sediments at Bucksport and Indian Point vary from predominantly fine to predominantly coarse over the study period. The median grain size of the bottom sediments at the Bridge Station site also varies between predominantly fine and coarse over the study period. The prevalence of ephemeral deposits of fine sediments at these sites indicates that the turbidity maximum migrates between Bridge Station and its landward limit, the Frankfort Flats reach.

The variability in bottom-sediment characteristics is likely due to the landward migration of the salt wedge as discharge decreases (Figure 20). As the turbidity maximum (salt wedge) migrates landward, bottom sediments at a fixed location would progress from coarse to fine and return to coarse if the landward extent of the turbidity maximum is farther upstream. The variability in bottom sediments at Bucksport and Indian Point reflect this progression (Figures 12-14). The variability in bottom sediments at Bridge Station deviates from this progression. This may be the result of cross-channel variability and a small change in station location. This may also be the result of a secondary turbidity maximum forming at this location, although there is not sufficient data to confirm this.

Secondary Circulation

The sediment collected at site WH 2 consists of over 80% fine sediments (Table 1). This deposit is not located within the thalweg in the Frankfort Flats reach, but in shallower waters at the break between the thalweg and the flats. Sediments in Marsh River, near the WH 2 site, are coarse and fine sediments are trapped within the thalweg near this location due to the likely presence of the turbidity maximum (Figure 14). The seemingly misplaced deposit of fine sediments at site WH 2 suggests that additional mechanisms exist that transport and trap sediments in the Frankfort Flats reach.

At the Frankfort Flats reach of the Penobscot River Estuary, the channel meanders through a right-handed bend followed by a left-handed bend, looking upstream, over a distance of approximately 5 km (Figure 15). The flow around these bends experiences a centripetal acceleration that drives surface waters towards the outside of the bend and near-bottom suspended-sediment rich waters towards the inside of the bend. During the flood, flow first travels around the right-handed bend, resulting in a secondary circulation that operates in a clockwise direction, looking upstream. During the ebb, flow first travels around the left-handed bend, resulting in a secondary circulation that operates in the opposite, counterclockwise, direction from the same orientation. The expected magnitude of the across-channel velocity of the bottom waters can be calculated by following Geyer, 1993 through a simplification of the expression for secondary circulation, resulting in the following equation:

$$\frac{C_D|u|v}{\tilde{h}} = \frac{u_s^2 - \overline{u_s^2}}{R} \qquad (7)$$

where C_D is the drag coefficient, equal to 3.0x10^{-3}, u is the along-channel (streamwise) velocity of the bottom waters, v is the across-channel velocity of the bottom waters, u_s^2 is a representative along-channel (streamwise) velocity value near the bottom, $\overline{u_s^2}$ is the depth-averaged square of the along-channel (streamwise) velocity throughout the entire water column, $\tilde{h}$ is the lower layer depth (about half of the water depth), and R is the radius of the meander (Geyer, 1993). The radii of the right-handed and left-handed bends are, respectively, 0.74 km and 1.20 km.

The expected magnitude of the across-channel velocity during flood currents ranges from 0.08 to 0.28 m/s based on the use of May or June data. Observed across-channel velocities during flood currents in May and June fall within this range, but do not reach the higher end of this range. Maximum observed across-channel velocities during flood currents are ~ 0.2 m/s (Figures 16, 17). The expected magnitude of the across-channel velocity during ebb currents is higher than that of flood currents, within the range of -0.45 and -0.52 m/s. Again, observed velocities do not reach this magnitude during the study periods. The observed across-channel velocities during ebb currents are ~ 0.2 m/s (Figures 18, 19).

During May and June, there is a convergence of bottom flow with a region of no flow, which results in an upwelling of water and settling of sediments. This convergence occurs at the location of site WH 2, where the seabed sediments are unconsolidated fine sediments. A tilt of the isohalines can also be associated with helical secondary circulation; however, sufficient observations for this structure in the water column in the Frankfort Flats reach of the estuary were not obtained. The isohalines seem to be primarily driven by ebbing or flooding waters, which create the convex upward structure as dense waters flood (Figure 16) or the convex downward structure as fresh waters ebb at the surface in the thalweg (Figure 18).

The sediment transport due to the secondary circulation created during flood and ebb currents can be analyzed through a calculation of the flux of suspended sediment through a plane perpendicular to the across-channel flow in the thalweg over a tidal cycle. The instantaneous flux, F, is represented as:

$$F = \int vc\, dz \qquad (8)$$

where v is the across-channel velocity (m/s), c is the concentration (mg/L), and dz is the depth interval. The instantaneous fluxes of sediment at intervals through the tidal cycle can be averaged over time, resulting in a net flux of sediment over the tidal cycle, represented as:

$$F_{net} = \frac{1}{T} \iint vc \, dz \, dt \quad (9)$$

where T is total time in tidal hours, and dt is the time interval.

The instantaneous flux of suspended sediment in the lower water column due to across-channel flow indicates transport of suspended sediment towards the inside of the right-handed bend during flood currents (positive values), and transport towards the inside of the left-handed bend during ebb conditions (negative values) (Figure 28). Although secondary circulation due to curvature will always be in the same direction around a particular bend, the secondary circulation at site WH 2, a location between two adjacent meanders, changes direction with flood and ebb currents. The net flux of suspended sediment over a tidal cycle sampled in May is 7.17 x 10^3 mg/ms, directed towards the inside of the right-handed bend. The net flux of suspended sediment over a tidal cycle sampled in June is -768.9 mg/ms, directed towards the inside of the left-handed bend. This suggests that during data collection in May, flood currents were dominant because the net flux of suspended sediment is in the direction of the bottom flow due to secondary circulation around the right-handed bend. During data collection in June, the net flux is in the direction of the bottom flow due to secondary circulation around the left-handed bend, suggesting that ebb currents were dominant. The magnitude of the net flux of suspended sediment in May is much larger than the magnitude of the net flux in June. Additionally, the fine sediments found at site WH 2 in June are located where the net flux in the direction of the bottom flow due to secondary circulation around the right-handed bend would transport suspended sediments. The difference in magnitude and the location of fine sediments at WH 2 in June, despite the net flux being away from this location, suggest that the flow during flood currents around the right-handed bend drives the lateral flux of sediments in this system during low discharge conditions.

Comparison with Other Studies

Landward progression of the salinity intrusion with decreasing discharge has also been observed in the Merrimack River Estuary (Ralston et al., 2010) and the Hudson River Estuary (Geyer et al., 2001). This progression is also supported by observations by

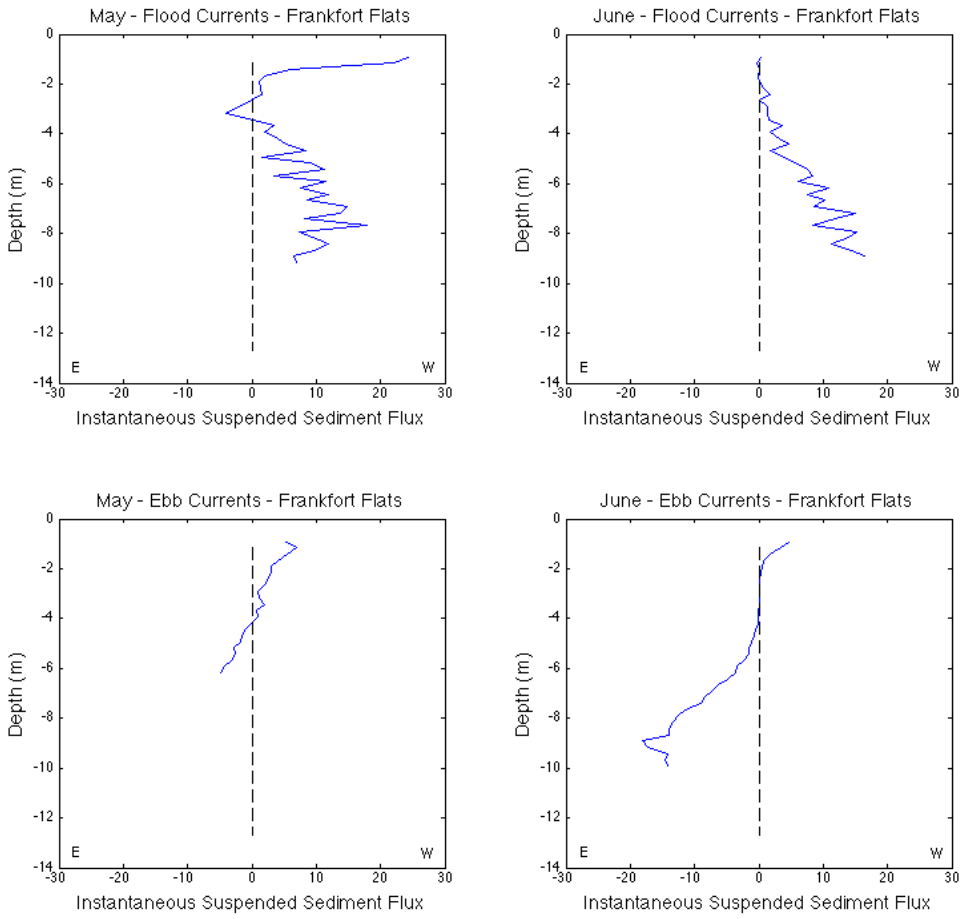

Figure 28. Instantaneous flux profiles in (mg/L*m/s) at maximum flood and ebb currents in May and June in the thalweg along the Frankfort Flats transect. The direction of the flux is determined by the direction of the across-channel velocity. Therefore, negative values represent flux to the east, when looking upstream, and positive values represent flux to the west from the same orientation.

Grabemann et al. (1997) that correlate a seaward migration of the turbidity maximum, often located near the landward extent salinity intrusion, with high discharge events, such as a freshet. Seasonal patterns of sediment deposition associated with the advection of the salt wedge, as exemplified in the Penobscot River Estuary, have also been observed in the Hudson River Estuary (Geyer et al., 2001) and the Gironde estuary (Migniot, 1971).

Importance

The trapping mechanisms associated with the salinity intrusion and secondary circulation patterns of the Penobscot River Estuary act to focus and localize contaminants that are bound to the fine sediments within the estuary. The highest concentrations of mercury within the estuary observed at Frankfort Flats are the result of trapping that likely exists at the landward extent of the salinity intrusion and secondary circulation due to curvature that transports resuspended and advected sediments from the thalweg to the banks of the channel. Locations with high concentrations of mercury can be correlated to the distribution of fine sediments on the sea bed of the Penobscot River Estuary.

Conclusions

- Upstream and downstream sources of sediment at Verona and Winterport, respectively, coupled with the large-scale salinity structure indicates the likely convergence of fine sediments located near the Frankfort Flats reach of the Penobscot River Estuary.
- The location of the salt wedge is largely dependent on the magnitude of river discharge. During the freshet in April 2010, the landward extent of the salt wedge was pushed seaward to the Frankfort Flats reach. With the decrease in discharge in the weeks and months following the freshet, the salt wedge progresses landward. Assuming a turbidity maximum accompanies the location of the landward extent of the salinity intrusion, a landward progression of fine sediments would be expected in the months following the freshet.
- Secondary circulation due to the curvature of the channel operates in this system in opposite directions with a magnitude of ~0.2 m/s in the bottom waters during flood and ebb currents due to the close proximity of two bends in the region of Frankfort Flats.

Literature Cited

Brown, E., et al, 1999. Waves, Tides, and Shallow Water Processes. Butterworth-Heinemann in association with The Open University, England.

Cameron, W.M. and Pritchard, D.W., 1963. Estuaries. The Sea (Ed. MN Hill), Vol. 2, Wiley, New York, 306-324.

Chant, R.J., 2010. Estuarine secondary circulation *in* Contemporary Issues in Estuarine Physics, Cambridge University Press, Cambridge, 100-124.

Davies, J.L., 1964. A morphogenic approach to world shorelines. Zeit. Geomorphol., 8: 127-142.

Davies, R.S., 1972. History of the Penobscot River: Its use and abuse. M.S. Thesis, University of Maine.

Dyer, K.R., 1997. Estuaries: A Physical Introduction (2nd Edition), John Wiley and Sons, Chichester.

Geyer, W.R., 1993. Three-Dimensional Tidal Flow Around Headlands. Journal of Geophysical Research, 98: 955-966.

Geyer, W.R., 1993. The Importance of Suppression of Turbulence by Stratification on the Estuarine Turbidity Maximum. Estuaries, 16(1): 113-125.

Geyer, W.R., 2010. Estuarine salinity structure and circulation *in* Contemporary Issues in Estuarine Physics, Cambridge University Press, Cambridge, 12-26.

Geyer, W.R., Woodruff, J.D., and Traykovski, P., 2001. Sediment Transport and Trapping in the Hudson River Estuary. Estuaries, 24(5): 670-679.

Grabemann, I., Uncles, R.J., Krause, G., and Stephens, J.A., 1997. Behavior of turbidity maxima in the Tamar (U.K.) and Weser (F.R.G.) estuaries. Estuarine, Coastal and Shelf Science, 45: 235-246.

Haefner, P.A., 1967. Hydrography of the Penobscot River (Maine) Estuary. J. Fish. Res. Bd. Canada, 24: 1553-1571.

Livingston, R.J., 2000. Mercury Distribution in Sediments and Mussels in the Penobscot River Estuary. Legal Proceedings: Maine People's Alliance and NRDC v. HoltraChem Manufacturing Co., LLC and Mallinckrodt Inc.

Maine Department of Economic Development, 1957. Development resources of the Penobscot region. Augusta, ME.

Middleton, G.V. and Southard, J.B., 1984. Mechanics of Sediment Movement. Society of Economic Paleontologists and Mineralogists Short Course Number 3 (2nd Edition). SEPM, Tulsa, 176-186.

Migniot, C., 1971. L'évolution de la Gironde ou cours des temps. Bulletin Institute Géologique Bassin d'Aquitaine, 11: 211-281.

Partheniades, E., 2009. Cohesive Sediments in Open Channels, Elsevier, Inc., Oxford.

Penobscot River Synthesis Project (PRSP), University of Maine, 2005. Html web site: www.pearl.maine.edu/windows/penobscot.

Ralston, D.K., Geyer, W.R., and Lerczak, J.A., 2010. Structure, variability, and salt flux in a strongly forced salt wedge estuary. Journal of Geophysical Research, 115.

Shorey, W.K., 1969. Macrobenthic Ecology of a Sawdust-Bearing Substrate in Penobscot River Estuary (Maine). J. Fish. Res. Bd. Canada, 30: 493-497.

Sternberg, R.W., 1972. Predicting Initial Motion and Bedload Transport of Sediment Particles in the Shallow Marine Environment *in* Shelf Sediment Transport: Process and Pattern, Dowden, Hutchinson and Ross, Inc., Stroudsburg, 61-82.

Traykovski, P., Geyer, W.R., and Sommerfield, C., 2004. Rapid sediment deposition and fine-scale strata formation in the Hudson estuary. Journal of Geophysical Research, 109.

Uncles, R.J., and Stephens, J.A., 1989. Distributions of suspended sediment at high water in a macrotidal estuary. Journal of Geophysical Research, 94: 14395:14405.

U.S. Federal Water Pollution Control Administration, 1967. Proceedings: Belfast, Maine April 20, 1967, Conference in the Matter of Pollution of the navigable waters of the Penobscot River and Upper Penobscot Bay and their Tributaries.

Valle-Levinson, A., 2010. Definition and classification of estuaries *in* Contemporary Issues in Estuarine Physics, Cambridge University Press, Cambridge, 1-11.

Appendix

-Velocity profiles for the thalweg throughout the tidal cycle for April (Figure A1), May (Figures A2a, A2b), and June (Figures A3a, A3b) flow conditions

-Velocity profiles for sites WH 1 (Figures A4a, A4b), WH 0 (Figures A5a, A5b), and WH 5 (Figures A6a, A6b) throughout the tidal cycle for June flow conditions

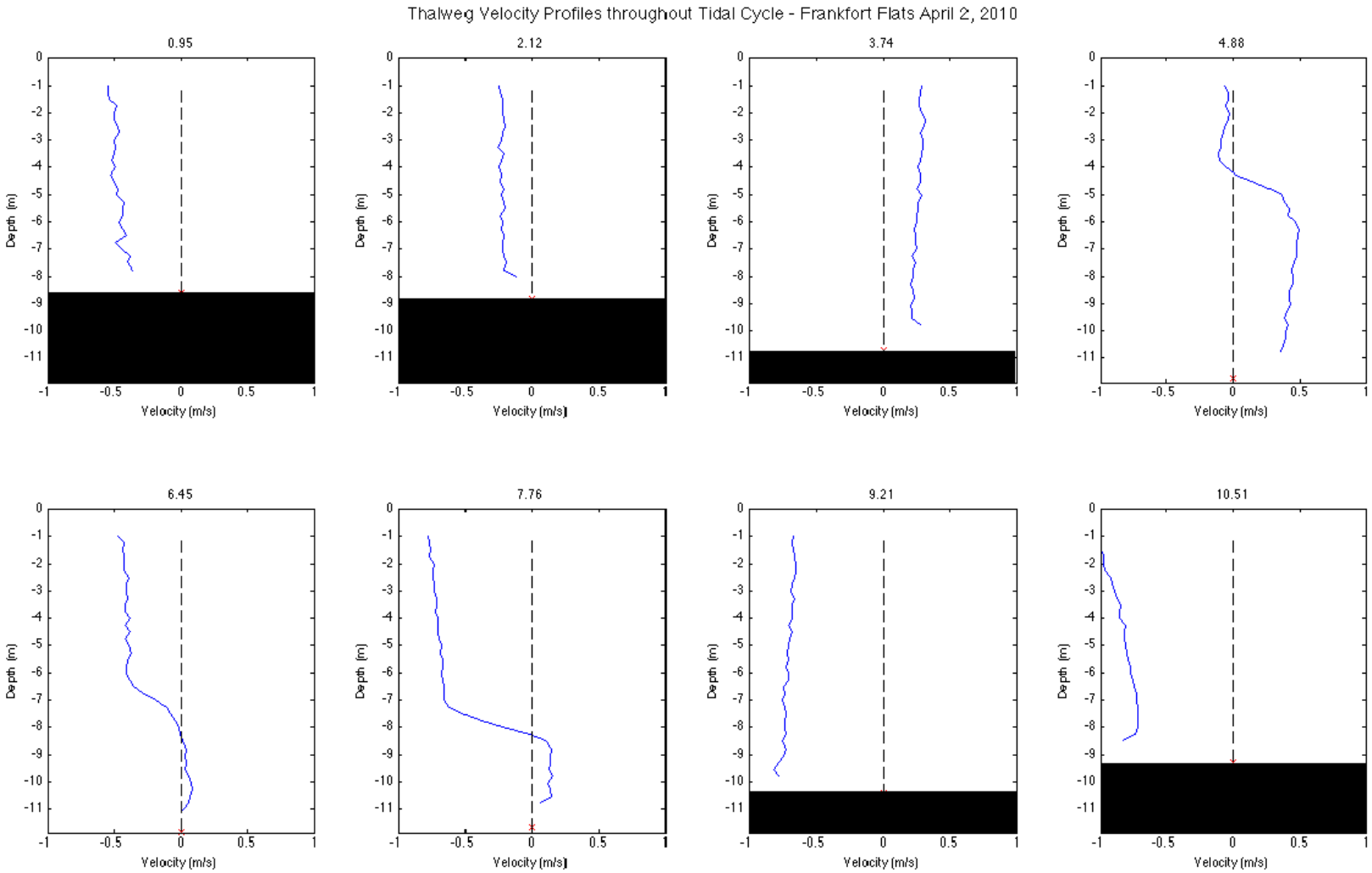

Figure A1. Mean velocity profiles in the thalweg during April throughout the tidal cycle. Tidal hour is noted at the top of each plot.

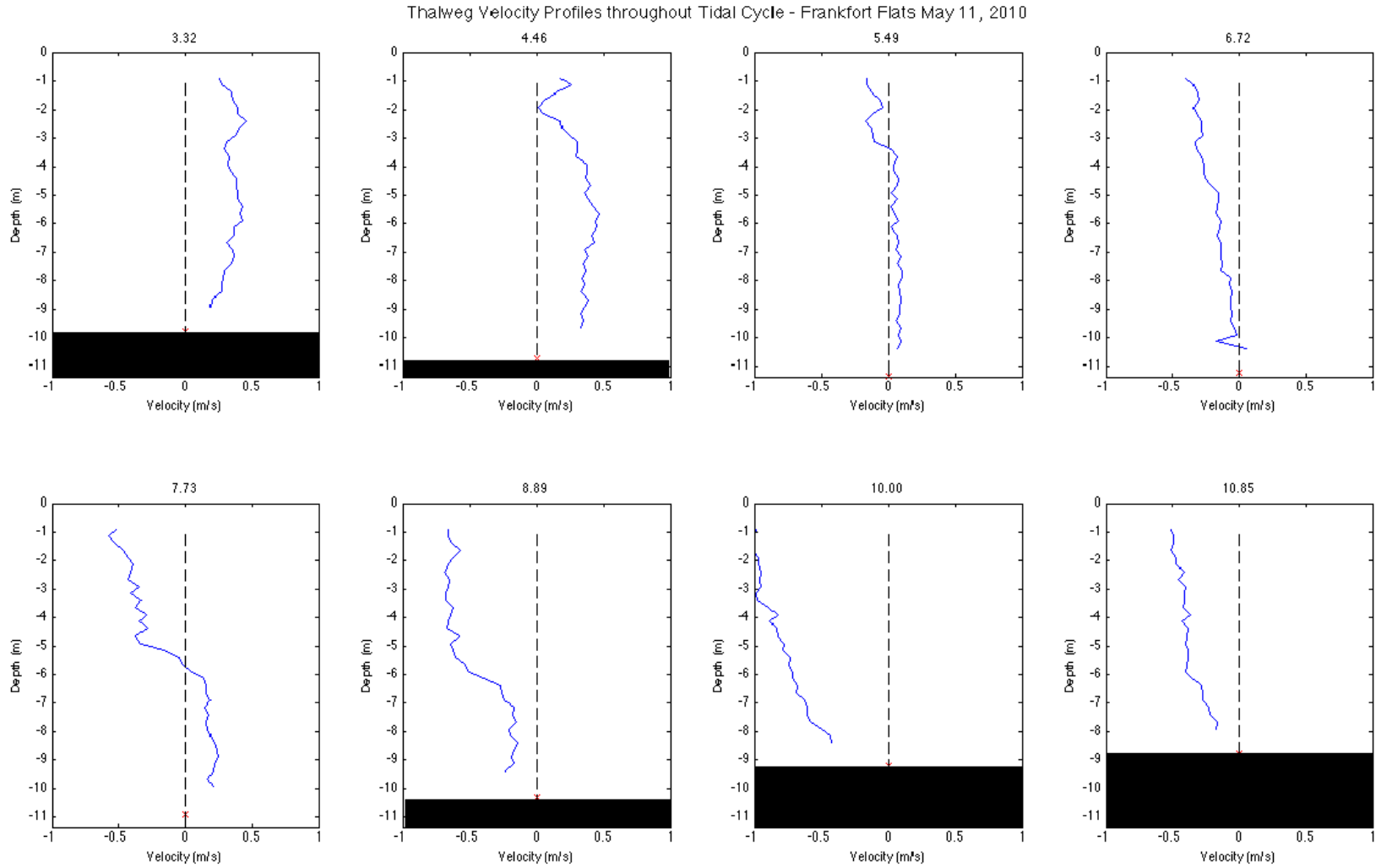

Figure A2a. Mean velocity profiles in the thalweg during May throughout the tidal cycle. Tidal hour is noted at the top of each plot.

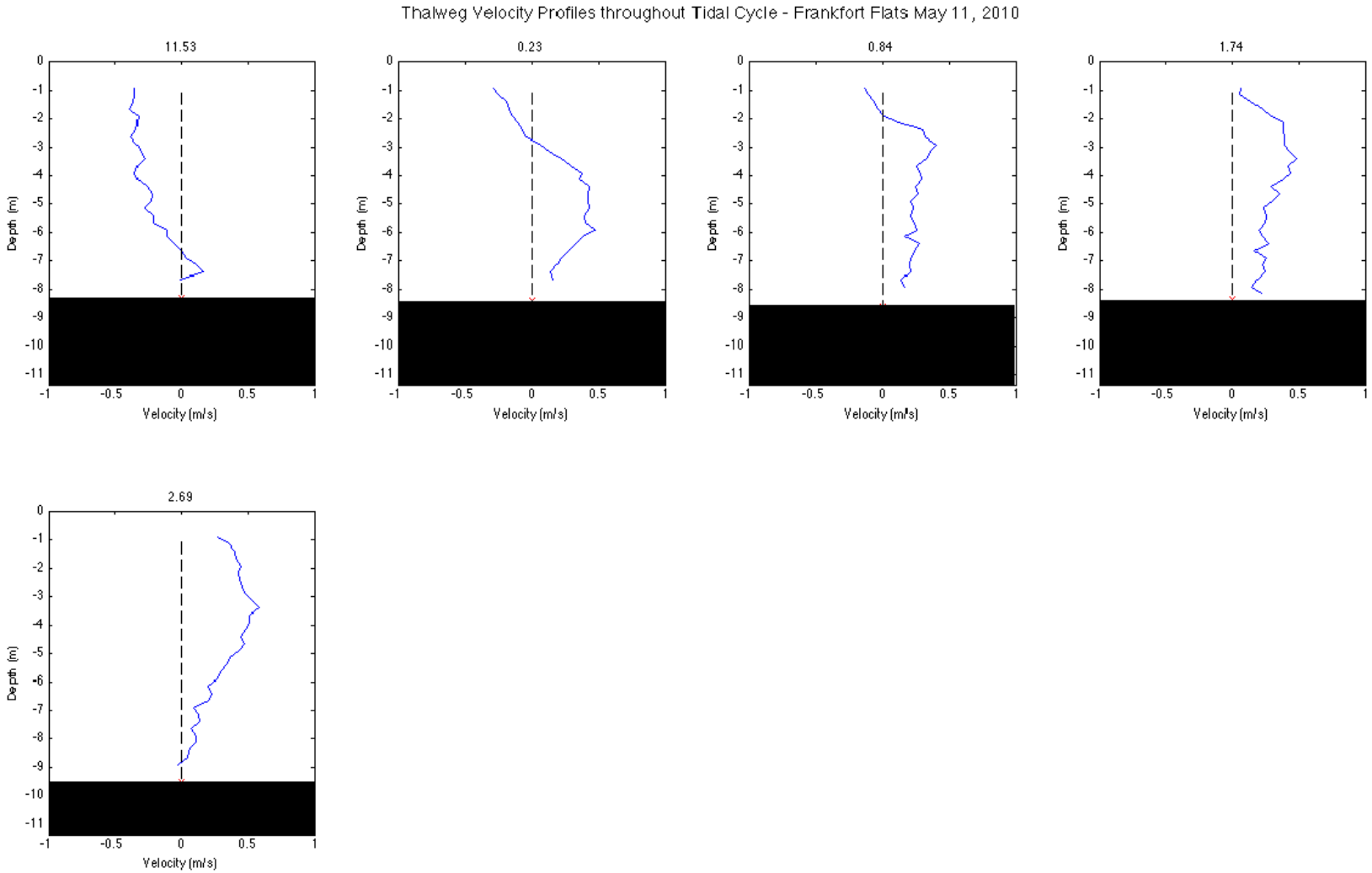

Figure A2b. Mean velocity profiles in the thalweg during May throughout the tidal cycle. Tidal hour is noted at the top of each plot.

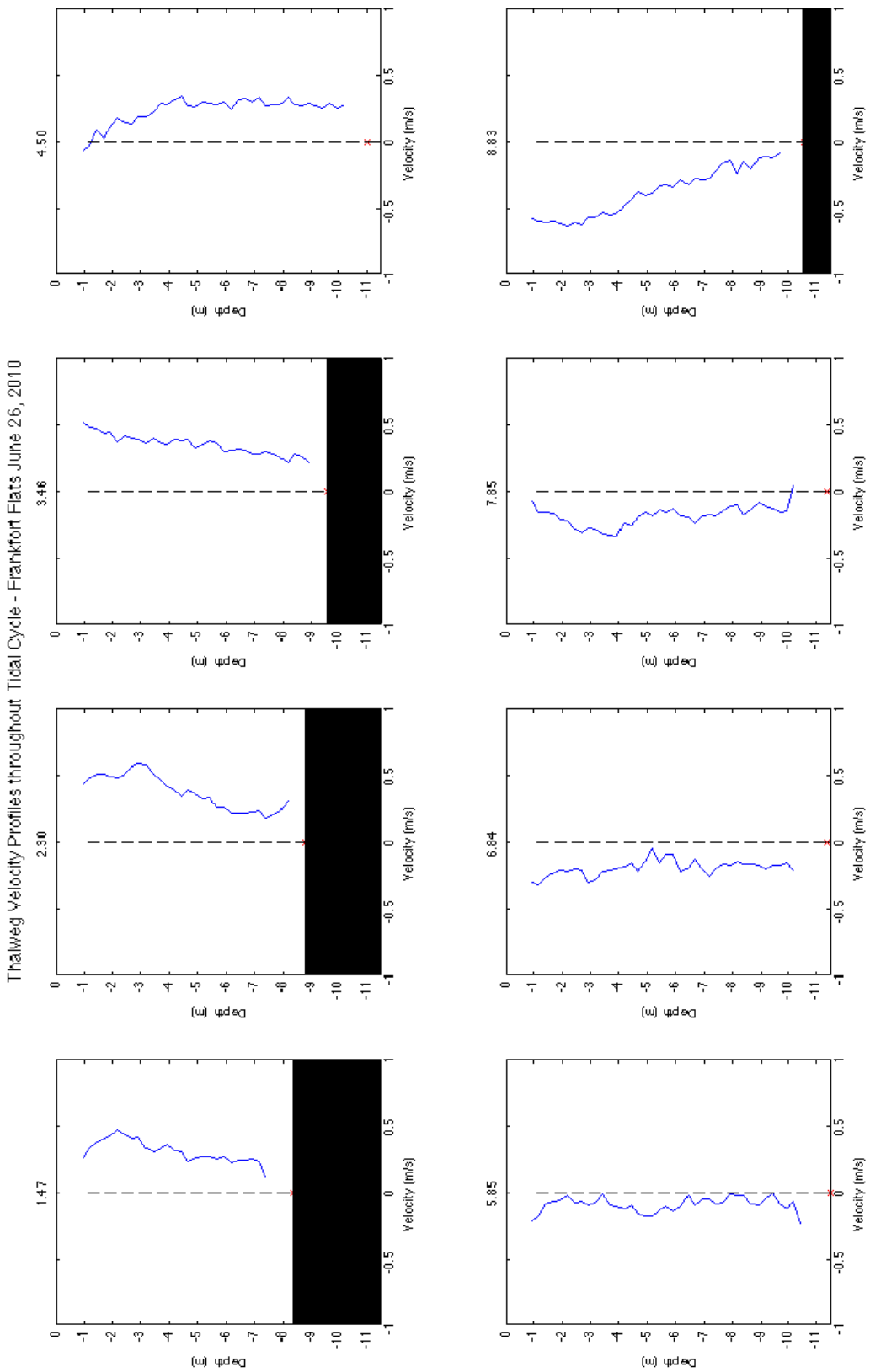

Figure A3a. Mean velocity profiles in the thalweg during June throughout the tidal cycle. Tidal hour is noted at the top of each plot.

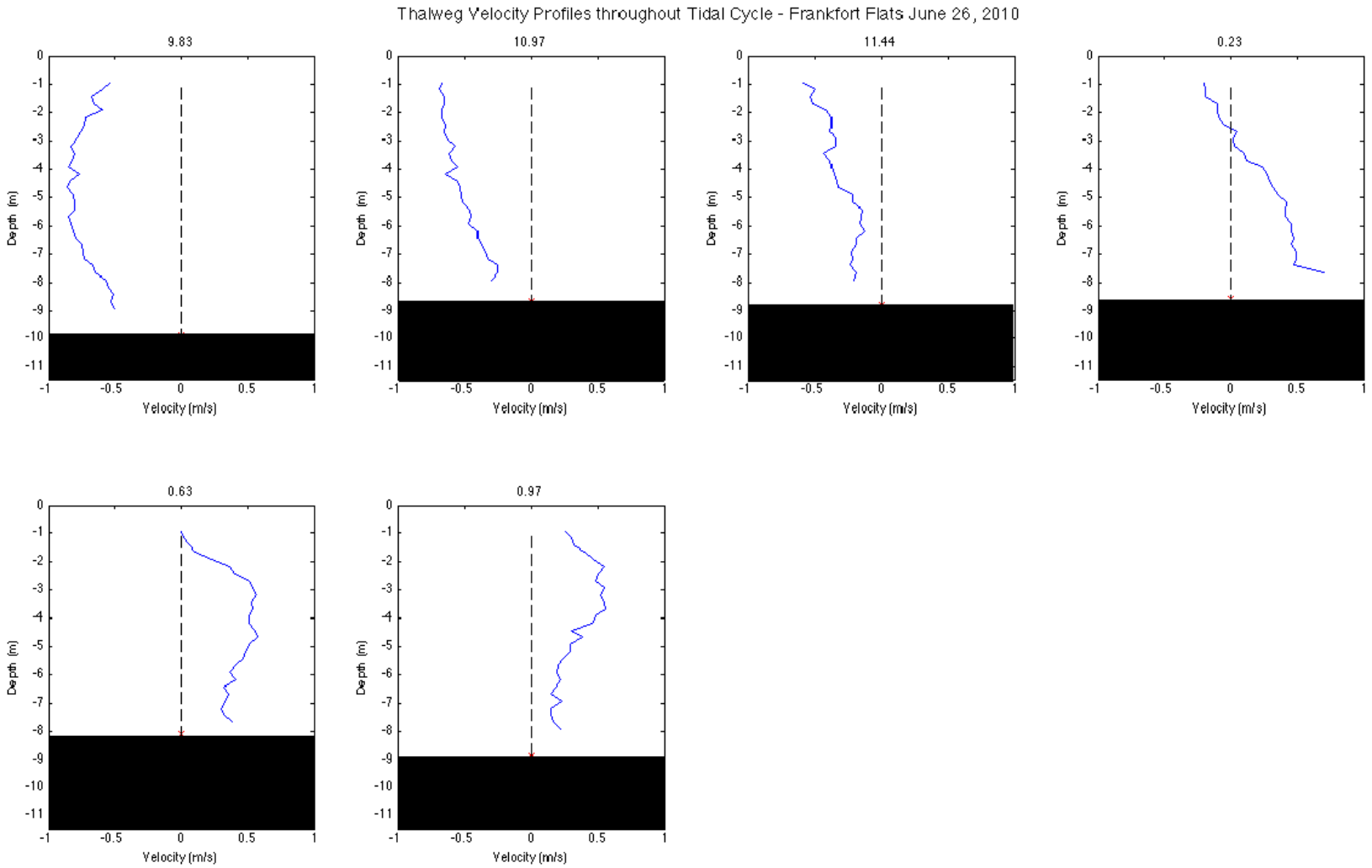

Figure A3b. Mean velocity profiles in the thalweg during June throughout the tidal cycle. Tidal hour is noted at the top of each plot.

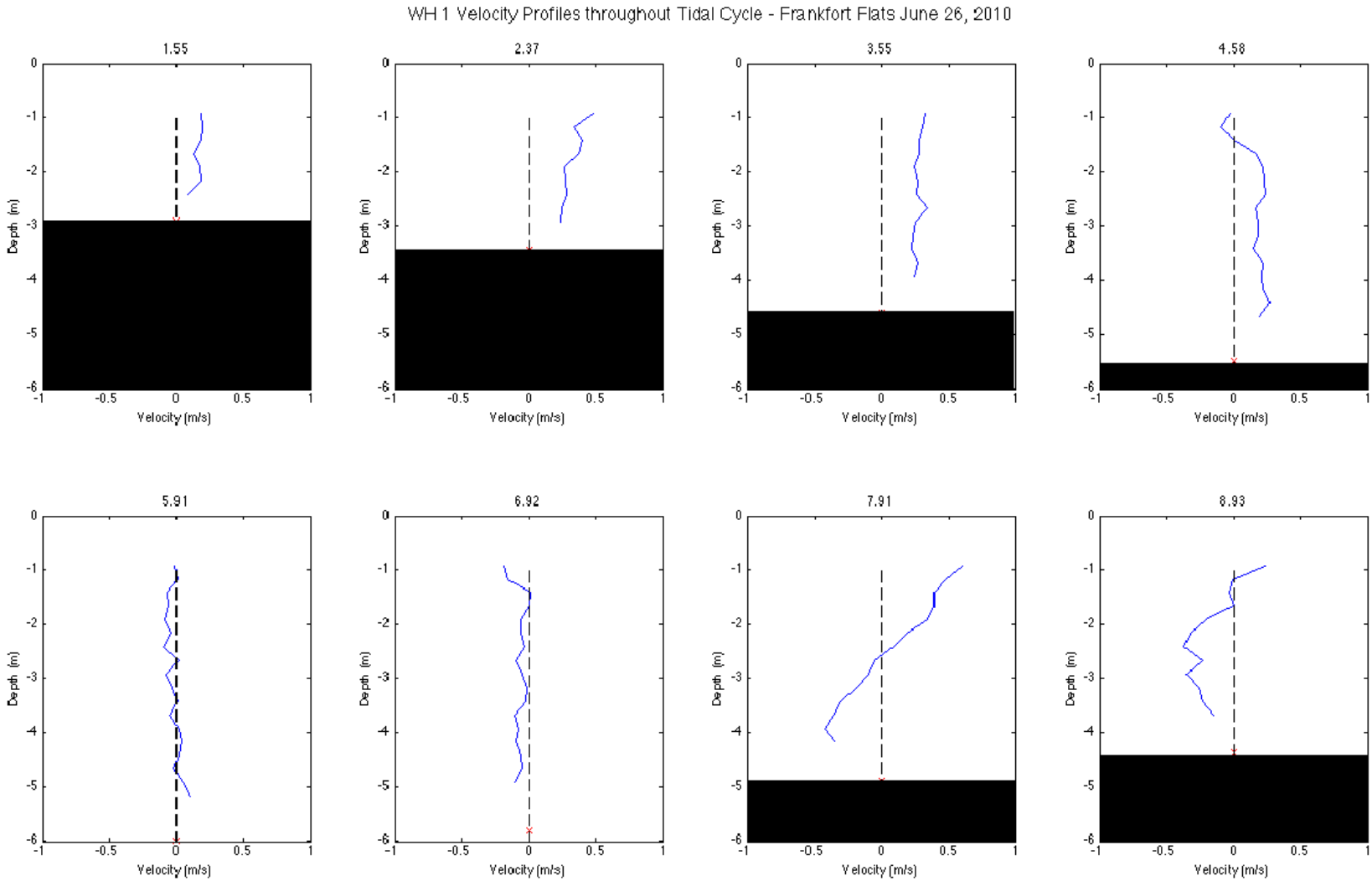

Figure A4a. Mean velocity profiles at site WH 1 throughout the tidal cycle. Tidal hour is noted at the top of each plot.

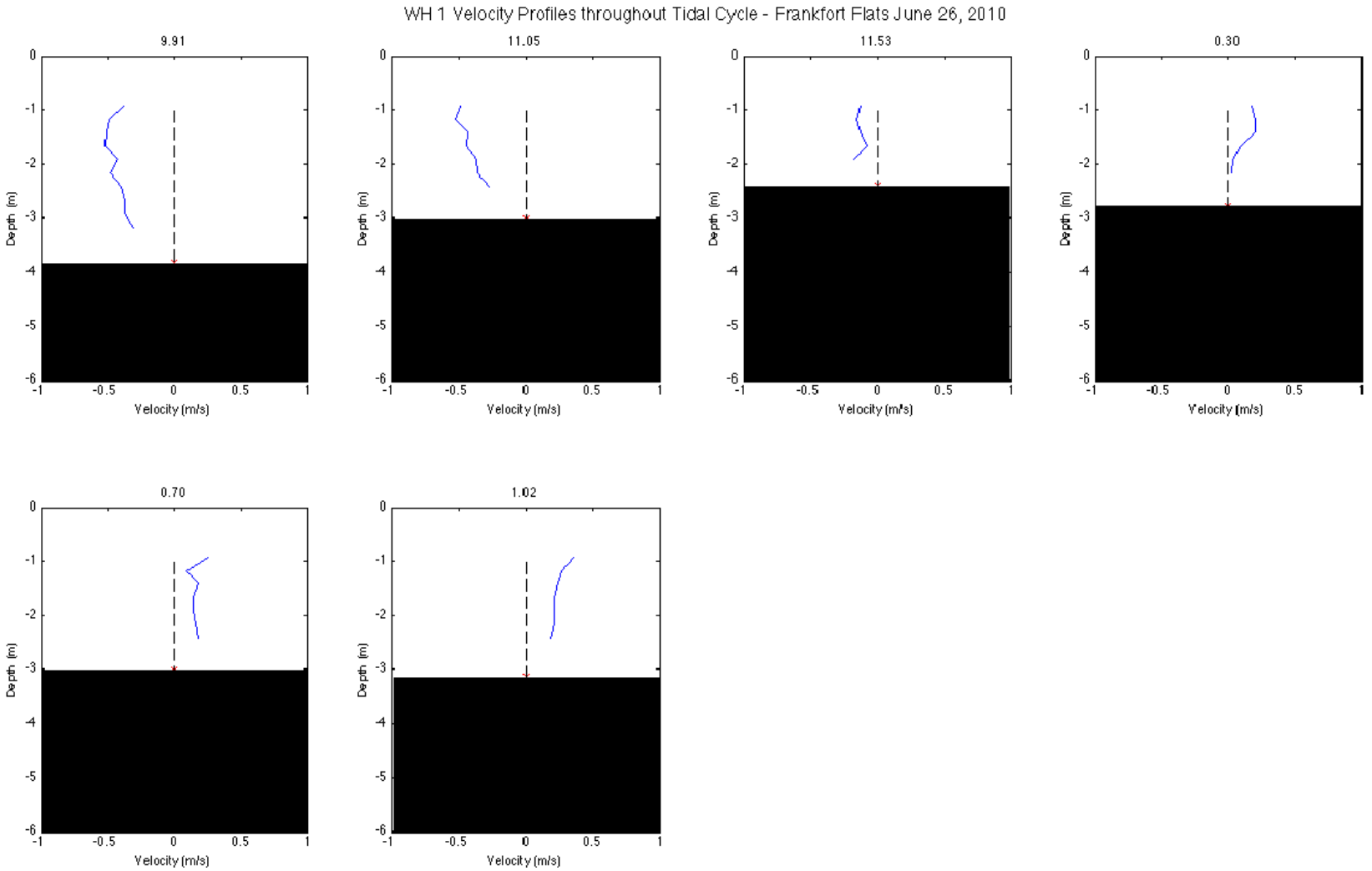

Figure A4b. Mean velocity profiles at site WH 1 throughout the tidal cycle. Tidal hour is noted at the top of each plot. Maximum velocity at one meter above the bed occurs during tidal hour ~11.00.

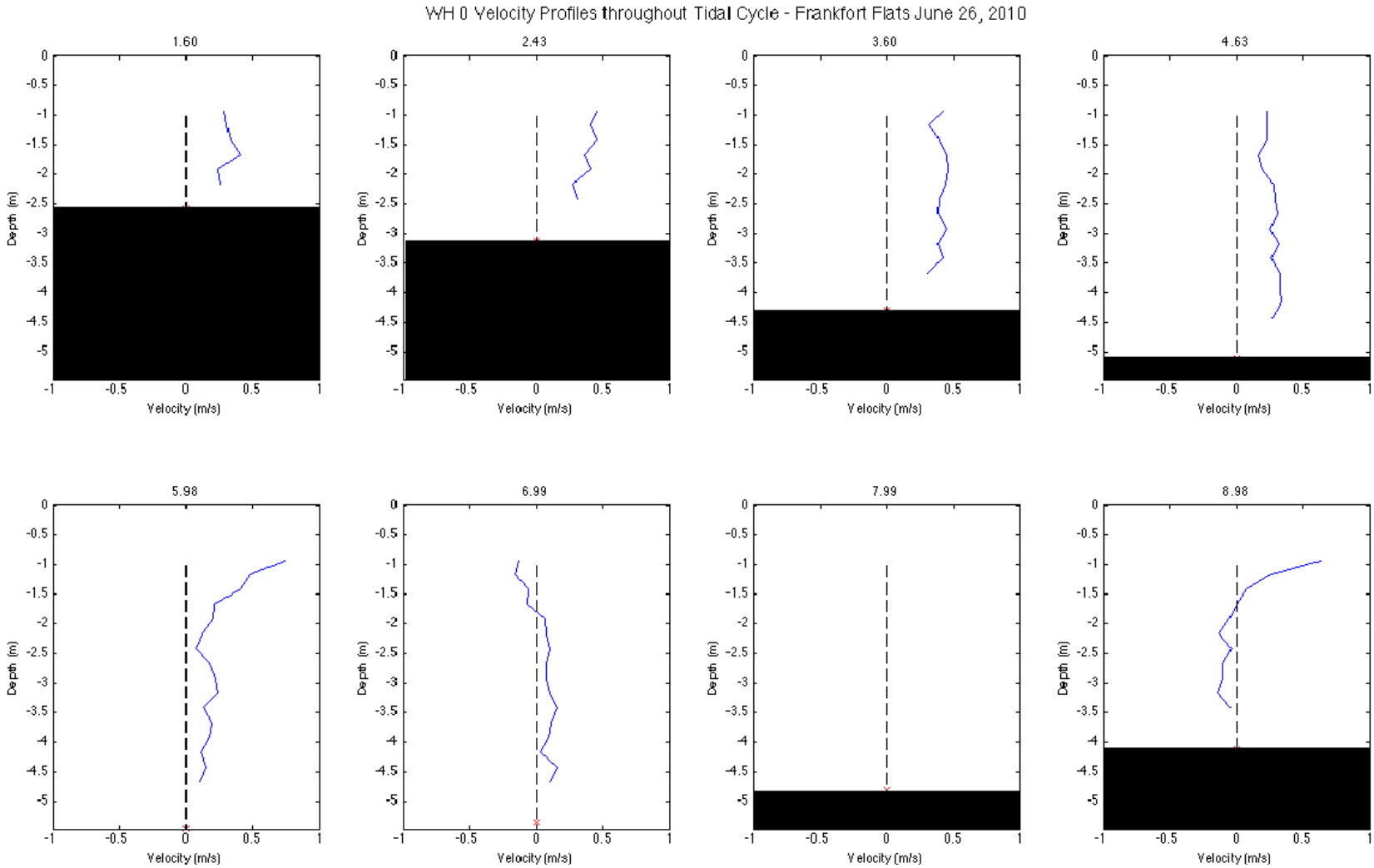

Figure A5a. Mean velocity profiles at site WH 0 throughout the tidal cycle. Tidal hour is noted at the top of each plot. Maximum velocity at one meter above the bed occurs during tidal hour ~3.60.

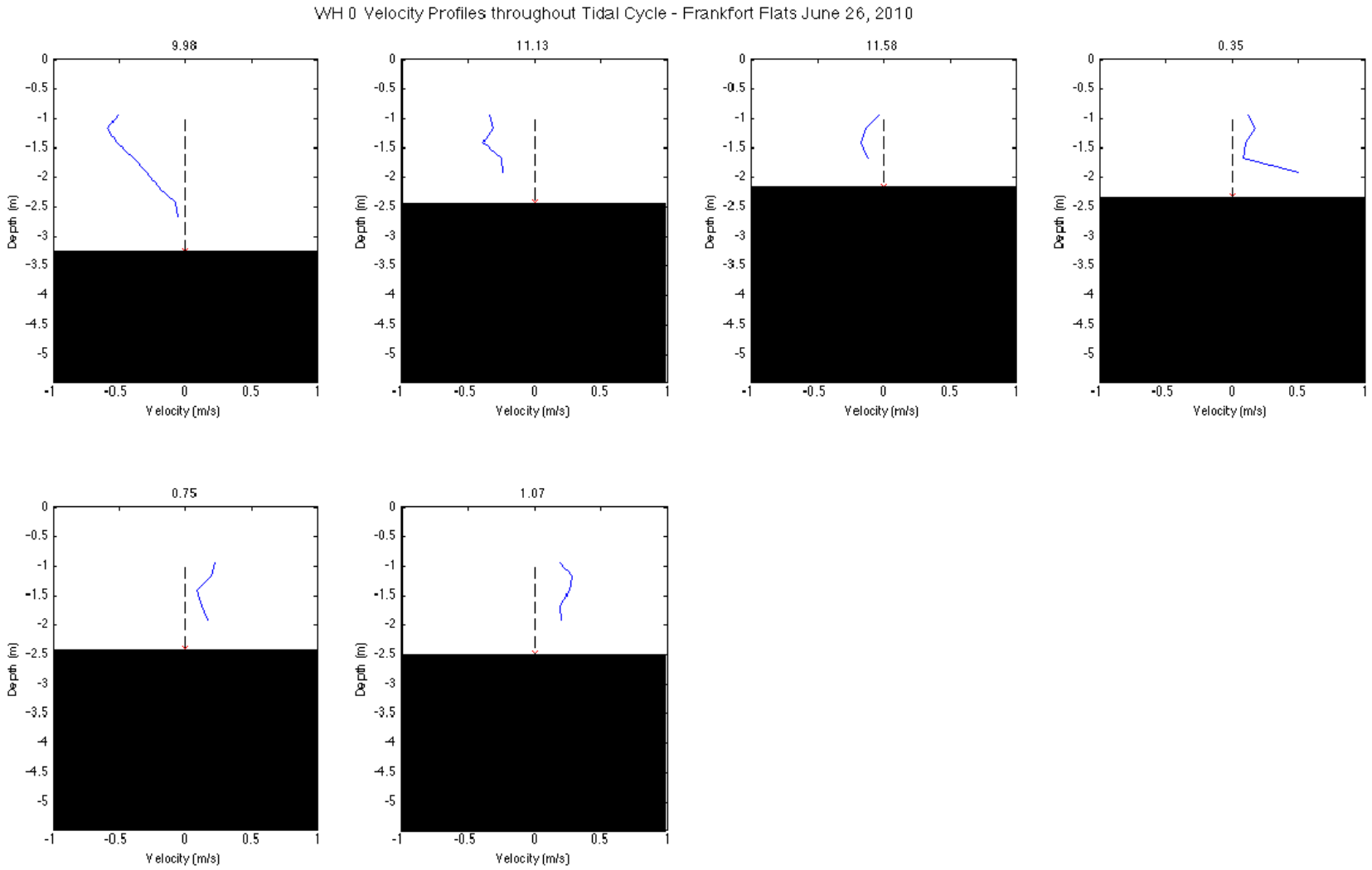

Figure A5b. Mean velocity profiles at site WH 0 throughout the tidal cycle. Tidal hour is noted at the top of each plot.

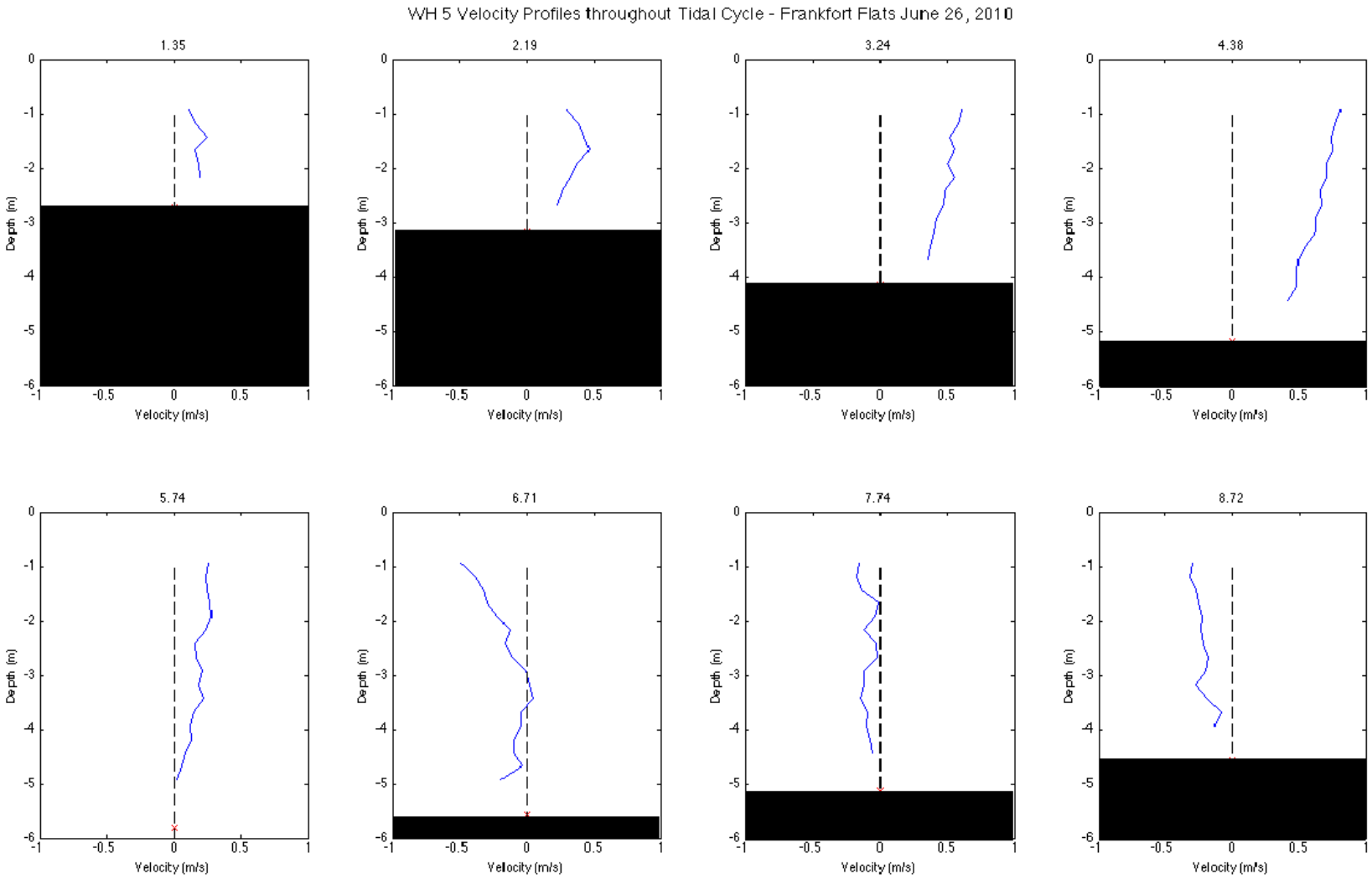

Figure A6a. Mean velocity profiles at site WH 5 throughout the tidal cycle. Tidal hour is noted at the top of each plot. Maximum velocity at one meter above the bed occurs during tidal hour ~4.38.

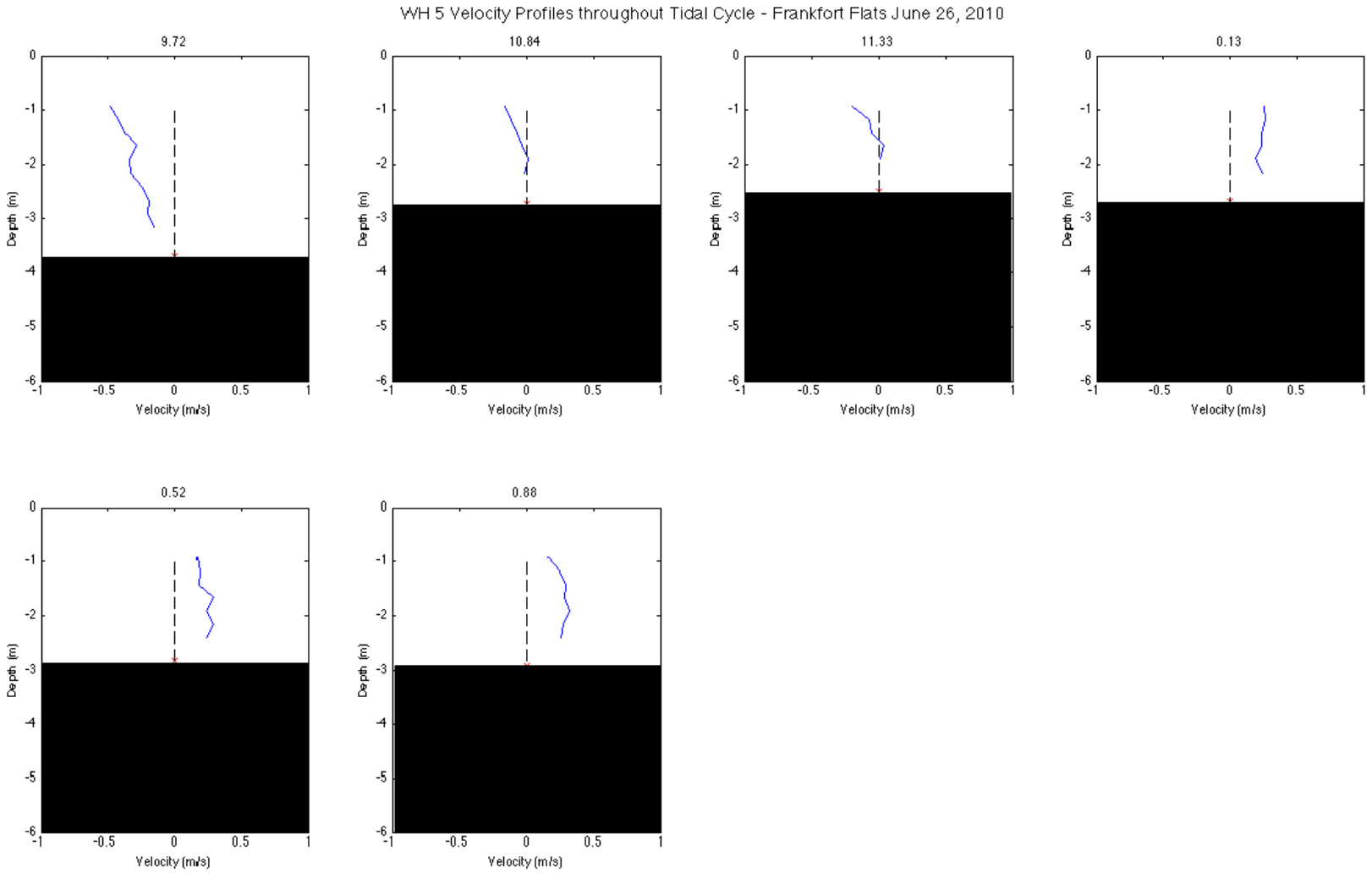

Figure A6b. Mean velocity profiles at site WH 5 throughout the tidal cycle. Tidal hour is noted at the top of each plot. Maximum velocity at one meter above the bed occurs during tidal hour ~11.